Applied Research Laboratory

Technical Report

DEVELOPMENT OF DAMPED METAL MATRIX COMPOSITES FOR ADVANCED STRUCTURAL APPLICATIONS

by

Clark A. Updike
Ram B. Bhagat

PENNSTATE

The Pennsylvania State University
APPLIED RESEARCH LABORATORY
P.O. Box 30
State College, PA 16804

DEVELOPMENT OF DAMPED METAL MATRIX COMPOSITES FOR ADVANCED STRUCTURAL APPLICATIONS

by

Clark A. Updike
Ram B. Bhagat

Technical Report No. TR 90-004
April 1990

Supported by:
Space and Naval Warfare Systems Command

L.R. Hettche, Director
Applied Research Laboratory

REPORT DOCUMENTATION PAGE

1a REPORT SECURITY CLASSIFICATION Unclassified	1b. RESTRICTIVE MARKINGS
2a SECURITY CLASSIFICATION AUTHORITY	3 DISTRIBUTION / AVAILABILITY OF REPORT Unlimited
2b DECLASSIFICATION / DOWNGRADING SCHEDULE	
4 PERFORMING ORGANIZATION REPORT NUMBER(S) TR-90-004	5 MONITORING ORGANIZATION REPORT NUMBER(S)
6a NAME OF PERFORMING ORGANIZATION Applied Research Laboratory Penn State University 6b OFFICE SYMBOL (*If applicable*) ARL	7a. NAME OF MONITORING ORGANIZATION
6c ADDRESS (*City, State, and ZIP Code*) P.O. Box 30 State College, PA 16804	7b. ADDRESS (*City, State, and ZIP Code*)
8a NAME OF FUNDING / SPONSORING ORGANIZATION Space & Naval Warfare Systems Command 8b OFFICE SYMBOL (*If applicable*) SPAWAR	9. PROCUREMENT INSTRUMENT IDENTIFICATION NUMBER N-0024-85-C-6041
8c ADDRESS (*City, State, and ZIP Code*) Department of the Navy Washington, DC 20363	10 SOURCE OF FUNDING NUMBERS PROGRAM ELEMENT NO. / PROJECT NO. / TASK NO. / WORK UNIT ACCESSION NO.

11 TITLE (*Include Security Classification*)
Development of Damped Metal Matrix Composites for Advanced Structural Applications

12 PERSONAL AUTHOR(S)
C.A. Updike, R. Bhagat

13a TYPE OF REPORT	13b TIME COVERED	14. DATE OF REPORT (*Year, Month, Day*)	15. PAGE COUNT
Technical	FROM _____ TO _____		96

16 SUPPLEMENTARY NOTATION

17 COSATI CODES			18. SUBJECT TERMS (*Continue on reverse if necessary and identify by block number*)
FIELD	GROUP	SUB-GROUP	damping, composites, metal matrix, structure, transverse vibration

19 ABSTRACT (*Continue on reverse if necessary and identify by block number*)

The development of damped metal matrix composite structures for advanced applications has been investigated by the use of two different approaches: (1) the development of metal matrix composites with high intrinsic damping compared to that of the matrix material, and (2) the development of coated metal matrix composites with high structural damping compared to that of the composite substrates. The two different approaches are analyzed in terms of their potential for improved damping and feasibility for structural applications. Damping was measured by the transverse vibration of free-free beams using the bandwidth technique by a laser vibrometer under ambient conditions. The damping measurements were made over a wide range of frequencies (.7 kHz to 25.6 kHz) at low strain amplitudes (10^{-10} to 10^{-7}).

Materials investigated for their tensile stiffness, strength, and damping

20 DISTRIBUTION / AVAILABILITY OF ABSTRACT	21. ABSTRACT SECURITY CLASSIFICATION	
☒ UNCLASSIFIED/UNLIMITED ☐ SAME AS RPT. ☐ DTIC USERS	Unclassified	
22a NAME OF RESPONSIBLE INDIVIDUAL	22b TELEPHONE (*Include Area Code*) 814/865-6344	22c. OFFICE SYMBOL ARL

performance include mechanically alloyed (MA) Al-Mg, SiCp/Al-Cu (MA), SiCp/Al, Al_2O_3(p)/Al, SiC_w/Al, planar random Gr/Al, unidirectional Gr/Al and unidirectional SiC(Nicalon)/Al composites. The effects of coatings of high damping metals (nitinol and incramute) on 6061-T6 Al and Al_2O_3(p)/Al substrates have also been studied. The measured damping is explained qualitatively in terms of transverse thermal current relaxation or intercrystalline thermal current relaxation. The effects of air damping and support losses are discussed.

The Al-Mg (MA), SiCp/Al (MA), SiC_w/Al and the Al_2O_3(p)/Al composites show no significant improvement in damping compared with that of the 6061-T6 Al. In contrast, the damping of Gr(planar-random)/Al, unidirectional Gr/Al and the unidirectional SiC/Al are about 12, 4 and 5 times that of aluminum, respectively. These composites were fabricated by high pressure infiltration casting. The damping of incramute coated aluminum is 25 times that of the aluminum substrate.

ABSTRACT

The development of damped metal matrix composite structures for advanced applications has been investigated by the use of two different approaches: (1) the development of metal matrix composites with high intrinsic damping compared to that of the matrix material, and (2) the development of coated metal matrix composites with high structural damping compared to that of the composite substrates. The two different approaches are analyzed in terms of their potential for improved damping and feasibility for structural applications. Damping was measured by the transverse vibration of free-free beams using the bandwidth technique by a laser vibrometer under ambient conditions. The damping measurements were made over a wide range of frequencies (.7 kHz to 25.6 kHz) at low strain amplitudes (10^{-10} to 10^{-7}).

Materials investigated for their tensile stiffness, strength, and damping performance include mechanically alloyed (MA) Al-Mg, SiC_p/Al-Cu (MA), SiC_p/Al, Al_2O_3(p)/Al, SiC_w/Al, planar random Gr/Al, unidirectional Gr/Al and unidirectional SiC(Nicalon)/Al composites. The effects of coatings of high damping metals (nitinol and incramute) on 6061-T6 Al and Al_2O_3(p)/Al substrates have also been studied. The measured damping is explained qualitatively in terms of transverse thermal current relaxation or intercrystalline thermal current relaxation. The effects of air damping and support losses are discussed.

The Al-Mg (MA), SiC_p/Al (MA), SiC_w/Al and the Al_2O_3(p)/Al composites show no significant improvement in damping compared with that

of the 6061-T6 Al. In contrast, the damping of Gr(planar-random), unidirectional Gr/Al and the unidirectional SiC/Al are about 12, 4 and 5 times that of aluminum, respectively. These composites were fabricated by high pressure infiltration casting. The damping of incramute coated aluminum is 25 times that of the aluminum substrate.

TABLE OF CONTENTS

LIST OF TABLES

LIST OF FIGURES

NOMENCLATURE

c	velocity of sound in air (344 m/sec)
C_p	specific heat at constant pressure
d	average grain diameter
E	Young's modulus
E'	the real part of the dynamic modulus
E''	the complex part of the dynamic modulus
f	frequency (Hertz)
f_1	the frequency below a resonance peak for which the response is half the response at resonance
f_2	the frequency above a resonance peak for which the response is half the response at resonance
f_n	the natural frequency of a structure
h	specimen thickness
k	Boltzman's constant
k_t	transverse thermal conductivity
L	length of specimen
M	mass of specimen
Q	activation enthalpy
Q^{-1}	inverse quality factor
R_r	radiation resistance
T	absolute temperature
W	width of specimen
α	linear coefficient of thermal expansion
$\Delta E/E$	relaxation strength or modulus defect
$\zeta = \xi$	damping ratio

η	loss factor
η_{oTTC}	relaxation strength of transverse thermal currents
η_{oICTC}	relaxation strength of intercrystalline thermal currents
η_R	damping due to radiation into air
η_{total}	total loss factor due to relaxations
ρ	mass per unit volume
$\rho_o c_o$	characteristic imedpance of air (440 kg/sec/m^2)
τ	relaxation time
τ_o	inverse frequency factor (or inverse attempt frequency)
τ_{ITTC}	relaxation time of transverse thermal currents
τ_{ICTC}	relaxation time of intercrystalline thermal currents
ν	Poisson's ratio
ϕ	loss tangent
ψ	specific damping capacity
ω	angular frequency (radians per second) = $2\pi f$

ACKNOWLEDGEMENT

We gratefully acknowledge the support of the U.S. Navy Space and Naval Warfare Systems Command.

Chapter 1

INTRODUCTION

1.1 Metal Matrix Composites

Much of the current efforts in advanced materials engineering is in the area of metal matrix composites (MMCs). MMCs have better high temperature strength and creep strength over that of unreinforced metals. MMCs also maintain or improve upon electrical conductivity, thermal conductivity, thermal dimensional stability of unreinforced metals.

MMCs can be made from a variety of matrices and reinforcements using a wide range of fabrication techniques. Some common metal matrices are aluminum, magnesium, titanium and nickel alloys. Reinforcements can be in the form of particulates, whiskers, discontinuous fibers and continuous fibers. Each form of reinforcement has its own advantages. Usually, it is easier to produce composites from smaller forms of reinforcement such as particulates. Reinforcement materials with high strength and stiffness are silicon carbide, graphite, alumina and boron.

Typically, MMCs are fabricated by liquid metal infiltration, P/M hot pressing or diffusion bonding. In liquid metal infiltration, molten matrix material is forced to infiltrate a fiber preform by applying pressure. Fibers are often coated to prevent excessive reaction with the molten matrix. This technique can be used to manufacture low cost

components. However, excessive fiber/matrix reaction frequently leads to poor mechanical properties. In P/M hot pressing, matrix powders and reinforcement are pressed at temperatures typically above half of the melting point of the matrix for prolonged periods of time. Unfortunately, a tradeoff occurs between densification of the matrix and the prevention of excessive reinforcement-matrix reaction. This makes it difficult to achieve good densification without causing excessive interphase formation. It is also difficult to use this technique with continuous fibers since hot pressing generally causes bending of the fibers which can lead to fiber breakage during the initial stages of pressing. Another limitation with P/M techniques is that they are costly. Diffusion bonding is similar to P/M hot pressing except that thin foils of matrix material are layered on fibers instead of the use of powders. As such, diffusion bonding techniques suffer from the same problems as P/M hot pressing, namely problems with densification, fiber breakage and cost.

Of the strengthening mechanisms available for metals, the only technique which will also increase the modulus is reinforcement with a high modulus material. In particular, continuous fiber composites have special advantages. In applications involving compressive or flexure loading, it is desirable to optimize E/ρ^2[1]. Since graphite fibers have densities lower than that of metal matrices, the density of graphite reinforced metal matrix composites decreases with increasing fiber volume fraction. For example, Gr/Al and Gr/Mg MMCs can be effectively utilized to optimize a design parameter involving stiffness and density.

1.2 Determination of Damping

Damping is the ability of a system to dissipate vibrational energy. For the case of forced vibrations, a useful measure of damping is the loss factor, η. η is the complex part of the dynamic modulus as expressed in (1.1):

$$E^*=E'+iE''=E'(1+i\eta) \text{ where } i=\sqrt{-1} \tag{1.1}$$

η can be calculated from the frequency response function by dividing the bandwidth , f_2-f_1, by the resonance frequency, f_n. The bandwidth is defined as the difference of the frequencies which dissipate one half of the energy dissipated at resonance. This is pictured in Figure 1.1. The derivation of the bandwidth technique can be found elsewhere [2]. There are also many other measures of damping. The equation below relates other measures of damping and the loss factor:

$$\psi=2\pi\tan\phi=2\pi\eta=4\pi\zeta=4\pi\xi=2\pi Q^{-1}=2\pi\frac{E''}{E'} \tag{1.2}$$

It should be noted that equation (1.2) is valid only when $\eta << 1.0$ which holds for metals and MMCs for which η is well below 1.0.

It is not always clear in the literature as to what type of damping is typically measured. Damping can generally be broken down into material damping and structural damping. Material damping is the damping a material inherently possesses and it is independent of structural geometry and usually strain amplitude. Structural damping is the damping that a structure possesses and it is geometry dependent and

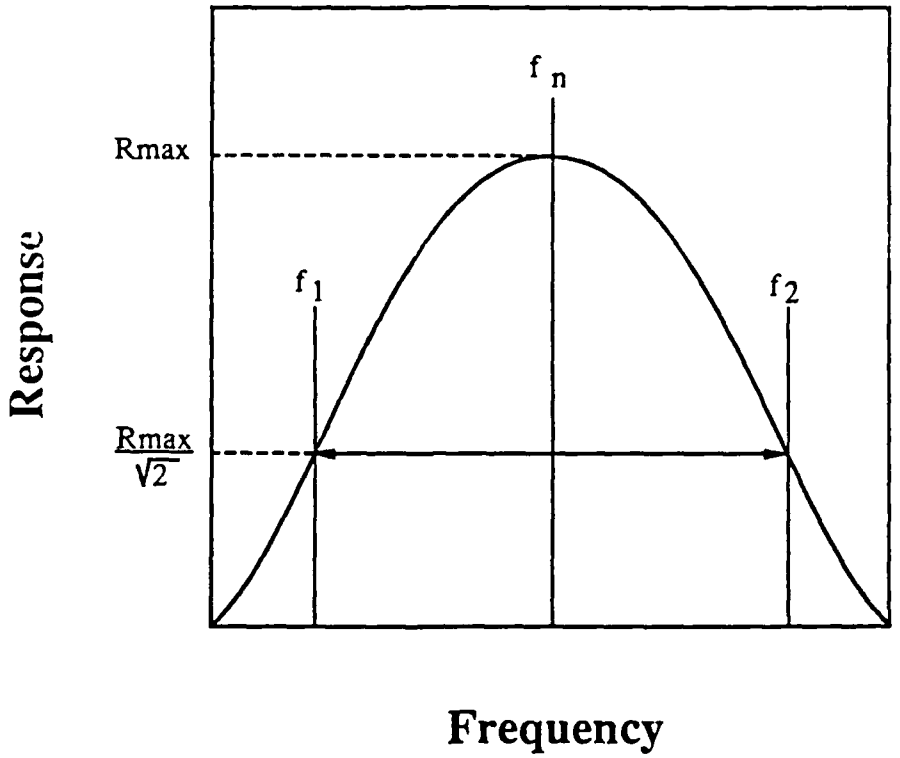

Figure 1.1 Schematic of the bandwidth (f_2-f_1) of a resonance peak

sometimes strain amplitude dependent. The measurement of structural damping always includes the material damping contribution. Ray et al. [3] claim that materials which have strain amplitude dependent damping must be tested by inducing a homogeneous strain field by a technique such as tension-tension fatigue. However, this notion disregards the elastic anisotropy of metals which is determined by the differences in elastic constants of different crystallographic orientations. This effect occurs in partially randomly orientated polycrystalline specimens. Zener [4] designates this elastic anisotropy factor as the R value of a metal that is in part responsible for the relaxation of intergranular thermal currents. Aluminum happens to be relatively elastically isotropic, which is why its damping is strain amplitude independent for amplitudes below about 10^{-5}. Further, Ray et al. state that tension-tension fatigue could be used to measure the material damping of a MMC since tension-tension fatigue produces a homogeneous strain field. However, the application of a tensile stress to a composite results in a complex network of strain gradients which is far from homogeneous. It is also claimed that flexural damping measurements can measure material damping only for strain independent materials such as aluminum. Based on the foregoing, the distinction between material damping and structural damping is not always clear and is for the most part unnecessary from a practical standpoint. For this reason, damping will be referred to as structural damping in order to distinguish it from systems damping, which involves the application of discreet damping devices. System dampers, such as dashpots, differ from structural

damping in that system dampers depend on the vibration amplitude of the point of application as opposed to the overall response of the structure [5].

1.3 Mechanisms of Damping

Any method by which a material dissipates vibrational energy can be a potential damping mechanism. This includes such nanoscale effects as solute pair reorientation and such macroscale effects as the flow of heat from one side of a specimen to another. Damping mechanisms can generally be broken down into relaxational mechanisms and non-relaxational mechanisms. A relaxation is a physical event in a material which dissipates vibrational energy and has a time period associated with it. This time is called the relaxation time and it must be a function of temperature. Usually, the relaxation time obeys an Arrhenius equation [2]:

$$\tau=\tau_o EXP(Q/kT) \tag{1.3}$$

Relaxations which obey the Arrhenius relation result in the Debye peak, schematically shown in Figure 1.2. This peak is defined as follows:

$$\eta=\frac{\Delta E}{E}\frac{\omega\tau}{1+(\omega\tau)^2}=\eta_o\frac{\omega\tau}{1+(\omega\tau)^2} \tag{1.4}$$

It is seen in Figure 1.2 that when $\omega\tau=1$, the Debye peak reaches its maximum. At $\omega\tau=1$, the damping from the relaxation reaches its maximum of one-half of the relaxation strength ($\eta=\frac{1}{2}\eta_o$). Relaxations are frequency and temperature dependent and strain amplitude independent, as

evidenced by equations (1.3) and (1.4) and are usually responsible for reported damping values. A resonance is similar to a relaxation in that a resonance is frequency and temperature dependent. However, a dislocation resonance does not obey equation (1.3) as does a true relaxation [6]. Non-relaxation mechanisms are relatively frequency and temperature independent and are strain amplitude dependent [7]. High damping metals possess non-linear mechanisms which are strain amplitude dependent. Interfacial friction is also a non-linear mechanism. Non-linear mechanisms usually result in higher damping than relaxations or resonances.

1.4 Applications Requiring High Damping

Often times a specific material application requires the optimization of two competing mechanisms. Damping is necessary to prevent large amplitudes of vibration which could lead to fatigue failure. Increased damping also leads to improvements in impact characteristics [8]. Materials with high strength and stiffness generally have low damping. For this reason, high damping coatings and constrained layer damping materials are used to improve the damping of a structure. However, some situations do not readily lend themselves to the use of these techniques. The application of high damping coatings might be prohibitively expensive or even technologically unfeasible. In these cases, it is desirable to increase the structural damping by increasing the damping of the base material itself. This technique thus avoids any problems associated with the use of an 'external' agent to

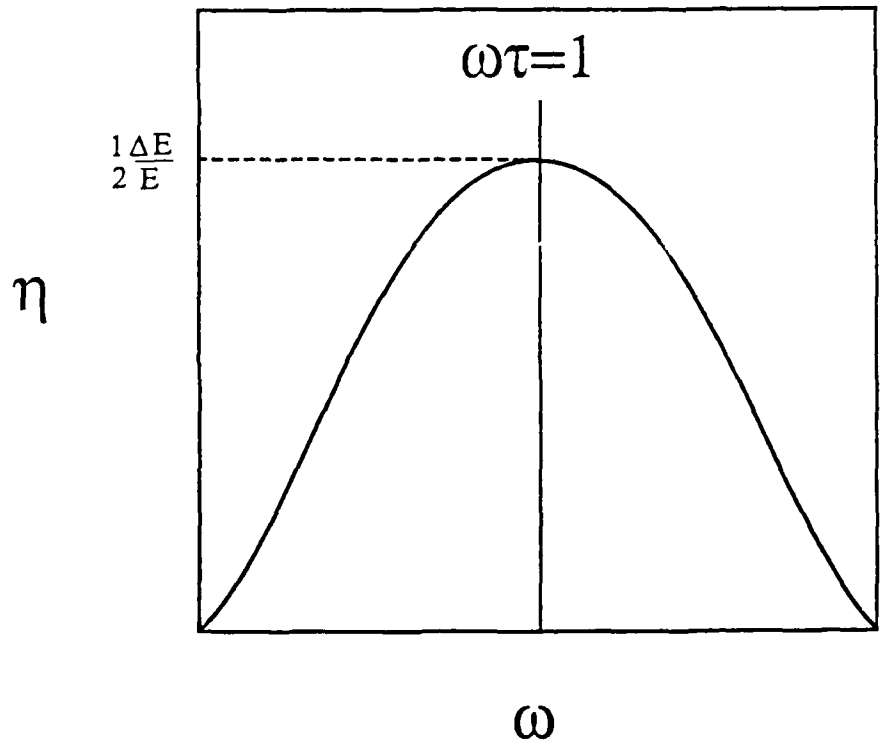

Figure 1.2 Schematic of a typical Debye peak

increase damping. MMCs show promise of demonstrating increased structural damping. The next section will present a review of some damping studies related to MMCs.

1.5 The Damping of MMCs

Research on the damping of MMCs is still in its early stage. It is difficult to draw conclusions from one researcher to another since damping measurements can be carried out over more than six decades of frequency using any one of several different measurement techniques. Further, one researcher will report damping as a function of temperature [9] while another will report damping as a function of frequency [10] and still another will report damping as a function of strain amplitude [11]. The lack of a standard for damping measurements makes it difficult to compare the results of one researcher with another.

DiCarlo and Maisel [12] used laminate theory to predict composite damping values from the relative amounts of constituent phases in the B/Al system. From this, dynamic behavior was predicted as a function of frequency, temperature and fiber volume fraction. Later, DiCarlo and Maisel [9] used a similar technique to predict the dynamic behavior of B/6061Al, B/1100Al, B(SiC)/6061Al, Al_2O_3/Al, SiC/Ti-6Al-4V and SiC/Ti composites. They suggested that this technique could be used to monitor fiber strength degradation due to processing. Wren and Kinra [13] found results consistent with a laminate theory for P55Gr/6061Al. They also found results for 6061Al which were consistent with the transport of transverse thermoelastic currents as proposed by Zener [4]. (This

thermal current relaxation mechanism is sometimes incorrectly referred to as Zener damping. However, Zener damping is the relaxation due the reorientation of solute pairs [2].) The composites which they tested showed negligible damping from the thermoelastic transport effect. They obtained reasonable predictions for the dynamic properties of Gr/Al composites using classical laminate theory based upon the work of Ni and Adams [14]. Rohatgi et al. [15] found that damping in graphite particulate reinforced composites increased with increasing volume fraction in a manner which was dependent on particle size, shape, particle/matrix bonding and fabrication technique. Crawley et al. [16] found that even at low stress levels, interfacial debonding and microcracking contribute to the damping. Further, they postulated that mobile dislocations generated by the large residual stresses in MMCs could lead to improved damping. Lee and Anderson [17] measured the damping of Gr/Al wires and found that the results correlated well with x-ray diffraction results. Kishore et al. [18,19] theoretically demonstrated a damping peak in low volume fraction composites due to interfacial slip caused by imperfect bonding. Their model showed a critical vibration amplitude above which static frictional forces between the fiber and the matrix could be overcome. Above this critical vibration amplitude, which depended strongly on the coefficient of friction between the fiber and the matrix, interfacial friction gave rise to increased damping. Töpler and Arnhold [20] found that damping increased linearly with dispersion content when Al_2O_3 and Al_4C_3 were reaction milled with an Al matrix. Bhagat et al. [21] measured the damping of planar random Gr/6061AL composites and found damping peaks

both as a function of volume fraction and frequency. Composite damping peaks were an order of magnitude over that of the matrix alloy. It was suggested that the damping peaks were due to microplasticity of the Al matrix and dislocation breakaway at the fiber/matrix interface. Bhagat et al. [10] also observed peak damping in a mechanically alloyed (MA) SiC_p/Al-Cu composite which was 2.8 times the damping of 6061-T6 Al.

1.6 Objective and Scope of the Investigation

The primary objective of this investigation was to develop new materials concepts for damped MMC structures with high strength and stiffness. Mechanical properties and damping data are to be presented and analyzed to provide insight into potential approaches for the development of damped MMCs. It was also intended that an attempt would be made to identify the underlying mechanisms responsible for the observed damping. Additionally, the investigation was aimed at developing a new experimental setup used to perform the damping measurements utilizing a non-intrusive laser vibrometer.

Chapter 2 will present the two different approaches which will be investigated for the development of damped MMCs. A description of the experimental procedure will be given in Chapter 3. Chapter 4 will provide a detailed analysis of the experimental setup. Measured damping data will be presented and analyzed in this chapter. Possible damping mechanisms will be proposed. Conclusions will be given in Chapter 5. Recommendations for future work will be described in Chapter 6.

Chapter 2

MATERIALS APPROACH TO IMPROVED DAMPING

Two different approaches can be taken to improve the structural damping of MMCs. One approach involves the use of an external agent, such as a high damping coating, to make up for the low damping of the base material. The other approach is to somehow improve the damping of the base material itself. Each of these approaches has pros and cons. These approaches must be evaluated on the basis of i) the mechanical properties resulting from each approach, ii) the integrity of the resulting structure, iii) the feasibility of producing the structure, and iv) the cost of producing the structure. The next two sections will consider the two different approaches for improving the damping of MMC structures in regards to the above criteria.

2.1 Improved Damping by an Extrinsic Approach

Substantial increases in structural damping can be achieved by the application of a high damping coating. Suitably heat treated high damping alloys such as nitinol (Ni-Ti) and incramute (Cu-Mn) have about 200 times the damping of typical engineering metals such as aluminum, titanium and nickel alloys [22]. The high damping of these metals is the result of non-linear mechanisms uncommon to everyday engineering metals [7]. As mentioned earlier, non-linear damping mechanisms generally are frequency and temperature independent but are strain amplitude dependent. This non-linearity is beneficial if the structure

must be damped for a range of frequencies and temperatures. However, this also means that these non-linear mechanisms often do not appreciably increase damping until a certain strain amplitude of vibration is achieved. It is important that the strain amplitude encountered in the application is high enough to significantly activate the non-linear mechanisms. Therefore, the increase in damping that the coating imparts to the structure depends on the strain amplitude to which the structure is subjected. This means that when a high stiffness substrate is used, there will be less of a damping contribution from the coating due to the correspondingly lower strain amplitudes. This strain amplitude dependence is particularly strong for peak damping of these metals at strain amplitudes greater than 10^{-6} [22]. In other words, it is likely that high damping coatings represent an 'all or nothing' situation. Either the application will have sufficient strain amplitudes to yield high damping or only modest improvements will be realized. Besides, the application of these materials presents some drawbacks. One drawback to these materials is that they all have relatively high specific gravity, typically over 7. For this reason, these high damping alloys should be used sparingly for lightweight advanced applications. A coating of these metals on a suitably undersized substrate could conceivably increase damping at a slight expense to the weight, specific strength and stiffness of the structure. A coating of a high damping alloy can be applied by techniques such as flame spraying or plasma spraying of powders made from high damping alloys. Another drawback is that the coating could induce large residual stresses due to differing coefficients of thermal expansion

coupled with high coating application temperatures. This will lead to warpage of the structure. Yet another drawback is that the coating is weakly bonded to the substrate. The coatings could chip off during machining. A heat treatment would be necessary to induce diffusion bonding between the coating and the substrate. However, the damping coating itself requires a heat treatment to achieve the high damping. It would therefore be difficult to optimize the damping of the coating without sacrificing the treatment necessary to produce diffusion bonding. This situation is further complicated by the fact that the substrate would also be affected by a heat treatment that is applied to the whole structure. It might be possible to apply a laser heat treatment [23] which would be localized in the coating. However, even if the difficulties of such a technique were surmounted, there is still no guarantee that the damping and bonding could both be maintained. Further, the coating and subsequent treatment would substantially increase the cost of the structure. These materials also could present problems with corrosion resistance [5]. Peak damping of high damping alloys can also be unstable due to natural aging as has been observed by Maksimov [24]. This peak damping instability could be significant if the application involves thermal cycling. However, it is possible that a significant increase in damping could still be achieved even without peak damping of the coating. Therefore, an increase in the damping of a structure can be realized by this technique if the aforementioned technological barriers can be overcome.

2.2 Improved Damping by an Intrinsic Approach

MMCs have demonstrated moderate increases in damping over that of the metal matrices themselves [21]. Therefore, it is possible that the need for a high damping coating can be eliminated by selection and tailoring of a suitable composite system. Composites can exhibit increased damping by introducing mechanisms of energy dissipation such as interfacial friction, effects of reinforcement or fabrication technique on grain size, dislocation damping mechanisms enhanced by large residual stresses, or simply by using a reinforcement which has higher damping than the matrix itself. One of the benefits from the use of uncoated MMCs is that the mechanical properties of the finished product are simply those of the bulk composite itself. This avoids the changes in the structure's mechanical properties which can occur when the structure is undersized, coated and treated to optimize the properties of the coating. The integrity of an uncoated MMC would also be better than that of one which is coated. An uncoated MMC would circumvent the problems of residual stresses and warpage associated with coating and eliminate the possibility that the coating could chip off. The cost of producing a damped, uncoated MMCs would be considerably less than that of producing coated MMCs for two reasons. First, much of the technology required to produce coated MMCs is still in its early stages and requires further development. Second, the coating technique is inherently expensive to carry out even if it were perfected since it requires undersizing, coating, surface treatment of the coating and subsequent heat treatment. The feasibility of producing damped

structures from MMCs is obviously better than that of coated MMC structures since the uncoated MMC structure is the initial building block of coated MMC structure. Further, MMCs can now be made by cost effective near net shape techniques which lower the structure's cost by reducing the amount of machining required. Uncoated MMCs suffer from two drawbacks compared with coated MMCs. One drawback is that MMCs with higher damping generally are less isotropic than lower damping composites. This means that coated substrates of lower damping MMCs would result in a more isotropic structure. Another disadvantage of uncoated MMCs is that they have less potential for increased damping than coated MMCs.

2.3 Selection of Materials

The materials selected for this investigation are chosen so that steps can be taken to develop both coated and uncoated MMC structures with significant damping. Table 2.1 lists the materials which have been used in the present investigation. The SiC_w/Al composite and the Al_2O_3(p)/Al composite are relatively isotropic but are likely to possess low damping [10]. They are candidates for the application of a high damping coating such as nitinol or incramute. The SiC_w/Al is manufactured by mixing SiC whiskers with the matrix powders. This mixture is then raised above the melting point of the matrix and is pressed. The high processing temperature promotes densification at a relatively low pressure. The composite is then extruded. The Al_2O_3(p)/Al composite is made by mixing the Al_2O_3 particulates into the

Table 2.1 Materials Selected for Evaluation of Damping

Materials:	**Source:**
Monolithics:	
6061-T6 Al	
6061Al (as cast, HiPIC)	this investigation
Al-Mg (MA)	Novamet
Nitinol	
Incramute	Incra
Composites:	
Particulate Reinforced:	
$Al_2O_3(p)/Al$ (V_f=0.15)	Dural
SiC_p/Al-Cu (MA) (V_f=0.15)	Novamet
SiC_p/Al (V_f=0.15)	Kaiser Aluminum
Whisker Reinforced:	
SiC_w/Al (V_f=0.20)	ACMC
Fiber Reinforced:	
SiC/Al (V_f=0.20)	this investigation
Gr/Al (V_f=0.21)	this investigation
Gr(p-r)/Al ($0.07 \leq V_f \leq 0.27$)	this investigation
High Damping Coatings:	
Unalloyed Nitinol	Astronautics Inc.
Unalloyed Incramute	Astronautics Inc.
Alloyed Nitinol	Astronautics Inc.
Alloyed Incramute	Astronautics Inc.

molten matrix followed by casting and extrusion. Both materials require extensive machining in order to produce parts from them. The $Al_2O_3(p)/Al$ composite fabricated by a recently developed, less costly, conventional casting technique. The planar random Gr/Al and the unidirectional Gr/Al and SiC/Al were made at The Pennsylvania State University. These composites were made by a low cost casting technique referred to as High Pressure Infiltration Casting (HiPIC) [25]. HiPIC uses high pressure to effect rapid infiltration of liquid metal into the fiber preform. This high pressure also acts to raise the solidification temperature of the metal thereby minimizing the molten metal-to-fiber contact time. This creates composites with a unique "clean" interface with minimal reaction products. Fiber-to-matrix bonding is of a primarily mechanical type. It is possible that the damping of these composites will be high enough to allow their use for damped structures without any high damping coatings [21].

The monolithic coating materials studied in this investigation are nitinol and incramute. Nitinol is a titanium-nickel high damping alloy while incramute is a copper-manganese high damping alloy. As mentioned earlier, both have densities about three times that of aluminum and damping about two hundred times that of aluminum for strain amplitudes above 10^{-5} [22]. Aluminum has been chosen as a reference material for this investigation. This is because aluminum is the matrix of the MMCs included in this investigation and the properties of aluminum are well established. Aluminum also possesses low damping. Hence, it is a good material for use as a standard in damping measurements since it indicates the sensitivity of the experimental setup. Mechanically

alloyed materials were investigated to determine whether or not they possessed high damping. Mechanically alloyed materials allow the combination of dispersion strengthening from oxide particles and a precipitation hardenable matrix. This previously unattainable combination of strengthening mechanisms must be made by the high energy ball milling of constituents which can't be combined using conventional metallurgical processes due to the reactivity of the constituents. The high energy ball milling homogenizes the powder mix by repeatedly welding and breaking the particles. The result is a powder which contains fine dispersoids within the alloy particles. The particles can then be consolidated using conventional techniques [26].

Chapter 3

EXPERIMENTAL PROCEDURE

This chapter will describe the experimental procedures which were carried out on the materials selected in this investigation. Details will be given on the method used to measure damping along with a description of the various equipment which were used. The procedure used to perform tensile testing will be described.

3.1 Damping Measurements

The damping measurement setup used a beam specimen in transverse bending with free-free boundary conditions. The loss factor was measured using a resonant dwell technique. Norwick and Berry [2], Read and Dean [27], and De Batist [6] describe several other different methods which can be used to measure damping.

Specimens for the damping measurements were prepared by cutting a rectangular beam specimen (sometimes referred to as a "reed" in the literature [4]) from a block or plate of the bulk material. Further machining was then performed down to specified shapes. Typical beam dimensions were 100mmx10mmx3mm, although other specimens from previous studies [10,21] were examined which were smaller. The variation in beam geometry generally changes the frequency range over which the damping measurements are made without affecting the damping values. Small samarium-cobalt rare earth magnets were attached to the end of the beam specimens to allow excitation of different modes since all modes have

antinodes at the end of a free-free beam. The mass of the samarium-cobalt magnets typically was less than 0.1% of the mass of the beam specimens. The node lines of a given mode were marked onto the beam specimen so that the specimen could be suspended with the supports at the node points for the mode of interest. This helped to prevent transmission of energy into the supports.

The experimental setup consists of a beam suspension system, an electromagnetic drive coil, a doppler laser velocity measuring device, and signal analysis equipment. The beam suspension system is pictured in Figure 3.1. It is primarily constructed from a non-magnetic stainless steel. The beam specimen is supported from fine silk threads which are suspended from soft springs which satisfy a free-free boundary condition. This configuration is designed to minimize support losses. The electromagnetic drive coil is a hand wound coil of copper wire which is positioned so that the samarium-cobalt magnet extends nearly inside the core of the drive coil. This is important because the magnetic field of the drive coil is constant within the core of the drive coil. Thus, the driving force is linear with the input signal since a close proximity of the coil core and the magnet is maintained. The low amplitudes of vibration (determined to be less than 5 micrometers) ensure that the magnet remains within the linear region of the drive coil. Signal detection is achieved with a laser vibrometer which uses an optical frequency doppler technique to provide a non-contact, real-time measure of the absolute velocity of the out-of-plane motion of a surface. This technique can detect vibration amplitudes down to 10 nm. This allows damping measurements to be made at very low vibration

a)

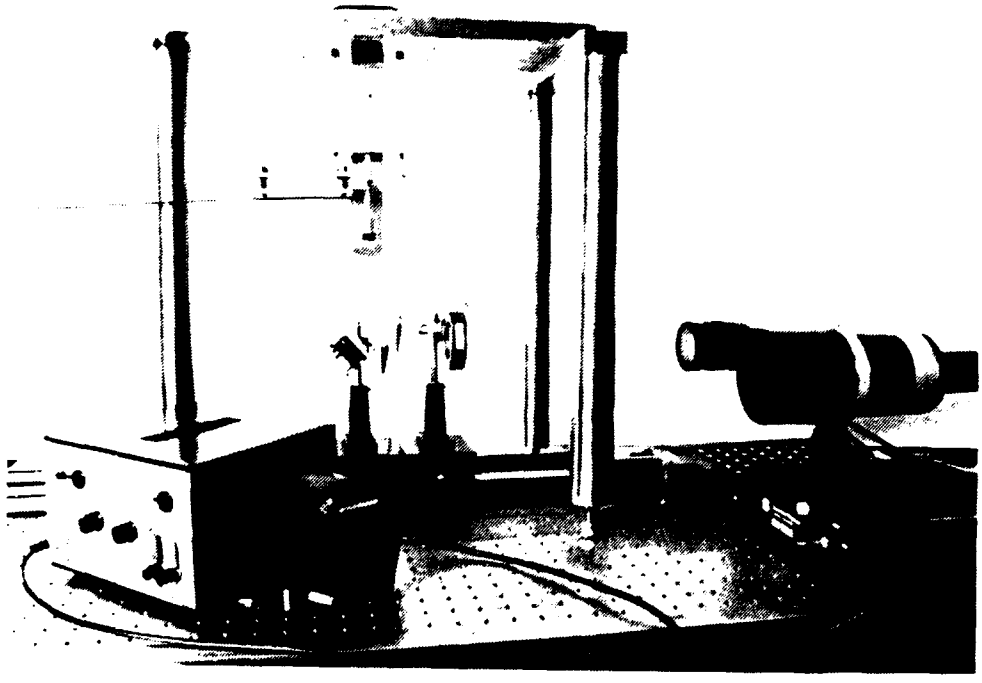

b)

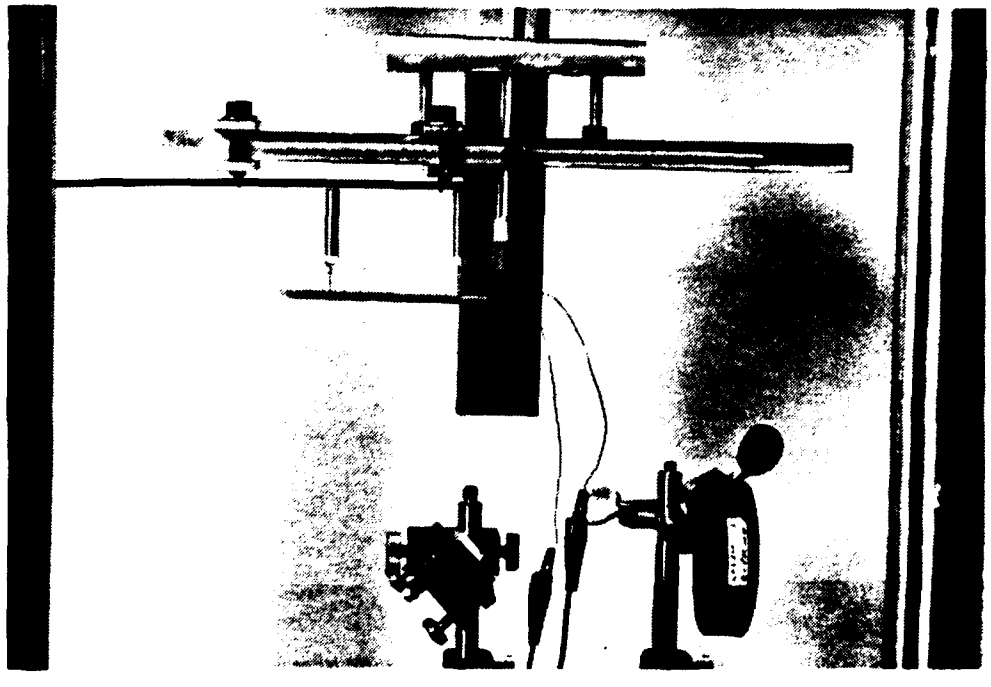

Figure 3.1 Photographs of the experimental damping measurement apparatus, a) the experimental damping measurement equipment, b) close-up showing the beam suspension system

amplitudes (less than 10^{-7} m). Output from the vibrometer is an analog dc voltage which can be directly related to the vibration velocity by a calibration factor. The calibration factor is dependent on the frequency range for which the vibrometer is set to measure. Signal analysis is performed by a dual channel analyzer linked to a computer with Structural Measurement System (SMS) software. The analyzer has a frequency range of 25.6 kHz. It also can "zoom in" on a given frequency range with window spans which are multiple half-intervals of 25.6 kHz. For example, it would be possible to look at a signal which lies between 3.2 kHz and 16 kHz by using a 12.8 khz window centered at 9.6 kHz. The frequency resolution of the analyzer is determined by the window size which can be as small as 1.56 Hz with a frequency resolution of 0.00195 Hz. The analyzer also has the capability to generate an excitation which matches the window which is being used. This is very useful for a resonant dwell measurement since individual modes can be precisely excited without exciting other modes. Typically, a random noise signal is sent from the analyzer's signal generator to the drive coil. The current through the drive coil is measured since it is proportional to the force generated by the drive coil. Therefore, the drive point mobility is measured to within a proportionality constant. The analog output from the vibrometer is input as the velocity to the analyzer. The transfer function designated H1 on the analyzer is used to measure the damping. H1 is the Fast Fourier Transform (FFT) of the ratio of the velocity signal to the drive signal. The first step in measuring the damping is to locate the resonance peaks of the beam specimen. This is accomplished by supporting the beam from an arbitrary position and

exciting the beam with broad band random noise. This excites the resonances in the beam specimen. These resonances can then be zoomed in on using a narrow band window and excitation. The frequency response function is then input into the SMS software which performs a polynomial curve fit using a least squares technique. The software then reports the resonance frequency, the half bandwidth and the damping ratio percentage. The damping ratio can then be converted to the loss factor using equation (1.2). The experimental damping measurement apparatus is shown schematically in Figure 3.2.

3.2 Tensile Testing

Tensile test specimens were first cut from a block or plate of bulk material and then machined into a typical dog-bone shape using diamond tools necessary for the machining of composites. The dogbones were then routed with a carbide bit using a jig designed to promote specimen failure within the gage length under tensile loading. Tensile specimen surfaces were polished using progressively finer silicon carbide paper up to a 600 grit to ensure that the specimen was free from surface damage. Strain gages were then mounted parallel to the load axis. Testing was carried out on an Instron testing machine using a crosshead speed of .508 mm/sec. Load versus crosshead displacement was recorded in addition to load versus strain.

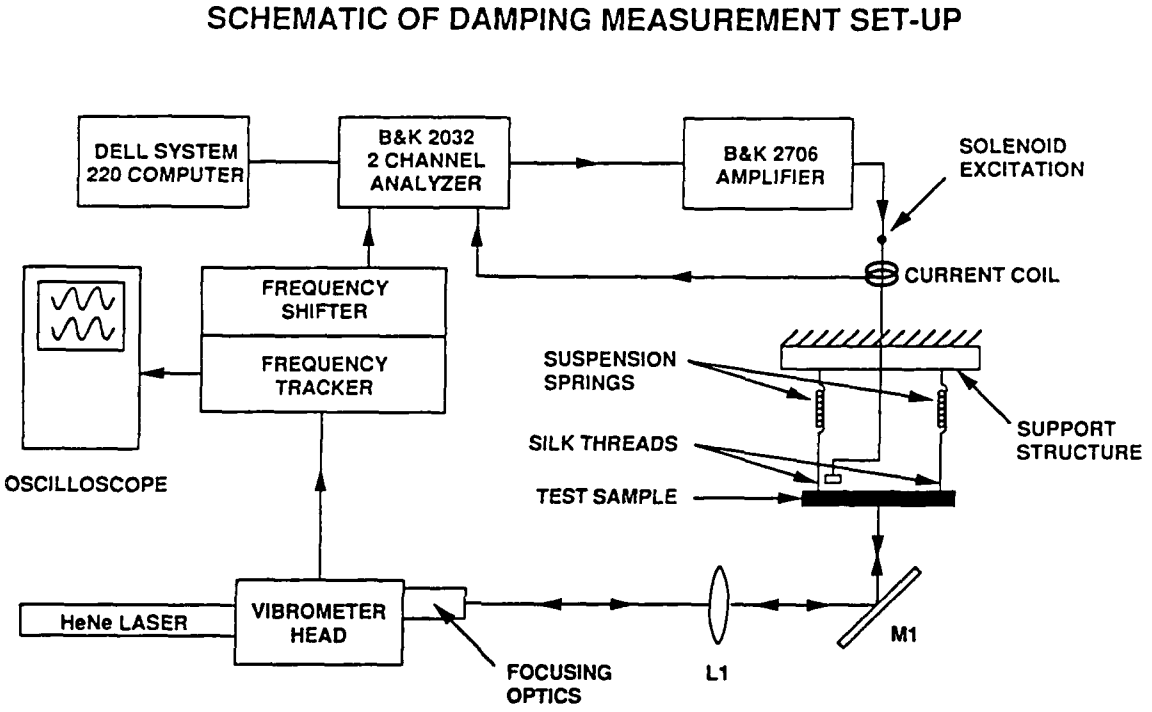

Figure 3.2 Schematic of the experimental damping measurement apparatus. The laser beam leaves the vibrometer head and is reflected off of the mirror onto the vibrating surface of the specimen. Part of the laser beam is reflected back into the vibrometer which then determines the specimen velocity based upon the doppler shift of the laser beam.

Chapter 4

RESULTS AND DISCUSSION

This chapter will present an in depth analysis of the experimental damping technique and will discuss factors which must be considered when evaluating the damping data. The materials concept development will then be analyzed in light of the damping results. This analysis will be broken down into the extrinsic and intrinsic structural damping approaches discussed earlier.

4.1 Verification Of The Experimental Damping Measurement

A free-free resonant dwell technique was chosen as the method for measuring damping. The use of a free-free technique eliminates clamping errors inherent to clamped-free boundary conditions. Read and Dean [27] stated that the bandwidth method was unsuitable for loss factors below about 10^{-2}. It was claimed that the bandwidth is too small to be accurately resolved below these values and that the free-decay method should be used for lower values. However, the bandwidth method has been used in this investigation to accurately measure loss factors below 10^{-4} without using the maximum resolution capability of the signal analyzer. The measurement technique has a maximum error of about 11% with a standard deviation of 5.1×10^{-6}. This was calculated by measuring the first mode of the 6061-T6 Al specimen. This specimen was selected because it has very low damping ($\eta = 1.4 \times 10^{-4}$). Ten trials were performed and after each trial the specimen was removed from the setup, replaced

and the vibrometer signal retuned. In this way, the error measured represents a maximum error since the beam does not have to be removed for each measurement. Also, this represents a maximum error since it is generally more difficult to measure low damping values. The error was calculated by taking the difference of the maximum value and the minimum value and dividing it by the mean. In practice, the error actually encountered in measuring a given mode is much lower than 11%. In fact, two measurements of a single mode were usually close enough to one another to provide reliable results. The primary cause of the error was due to the tuning of the vibrometer. The laser beam from the vibrometer had to be precisely focused on the specimen. It was found that the application of silver paint to the specimen greatly improved the vibrometer's signal. The vibrometer also had to be positioned at certain intervals from the specimen due to a characteristic of the laser known as the cavity length. Proper alignment of the lenses and mirrors also helped to insure a quality signal. The quality of the signal was monitored on an oscilloscope using the Monitor Out from the vibrometer. Care was required to ensure that only as much driving force was applied as was necessary since overly driven specimens would undergo rigid body motion and the vibrometer could lose its 'lock' on the specimen. Indeed, at higher frequencies where larger driving forces were required it was often difficult to find a driving force which would adequately excite the mode without causing excessive rigid body motion. Due to these problems, the strain levels achieved in this investigation represent somewhat of an upper limit of what can be achieved using a suspended free-free setup with a vibrometer. Despite all the effort to

prevent a loss of signal quality, in the course of taking averages poor coherence sometimes occurred. Selection of clean signals for curve fitting helped prevent unnecessary error. Further, visual inspection of the curve fit was used to screen potentially poor data. Figure 4.1 is the FFT of the first mode for the 7% Gr(p-r)/Al. Figure 4.2 is the data after it has been transferred to the SMS software and curve fit using a least squares polynomial fit. It can be seen from Figure 4.2 that the data and the curve fit agreed well, especially at the half-power points from which the bandwidth and damping were calculated. For the above reasons, the actual error in the measurement of a given mode was usually less than half of the 11% value which represents a worst-case scenario.

Whenever damping data are presented, it is necessary to consider just exactly what has been measured. This is because any source of extraneous energy dissipation which extracts energy from the specimen during the measurement will cause the measured damping to be greater than the structural damping of the specimen. There are several sources of extraneous damping which can lead to erroneous damping measurements for the resonant dwell setup used in this investigation. These factors are a) support losses, b) viscous losses and c) radiation losses. Support losses are the result of energy dissipation into the supports. It is difficult to quantify the magnitude of support losses. However, support losses were minimized by accurately supporting the fine silk loops at the node points of the specific mode. Furthermore, the specimens were seismically supported. Thus, the losses due to energy transfer through the supports to the base structure were minimized. Since anisotropic materials were investigated, efforts were made to

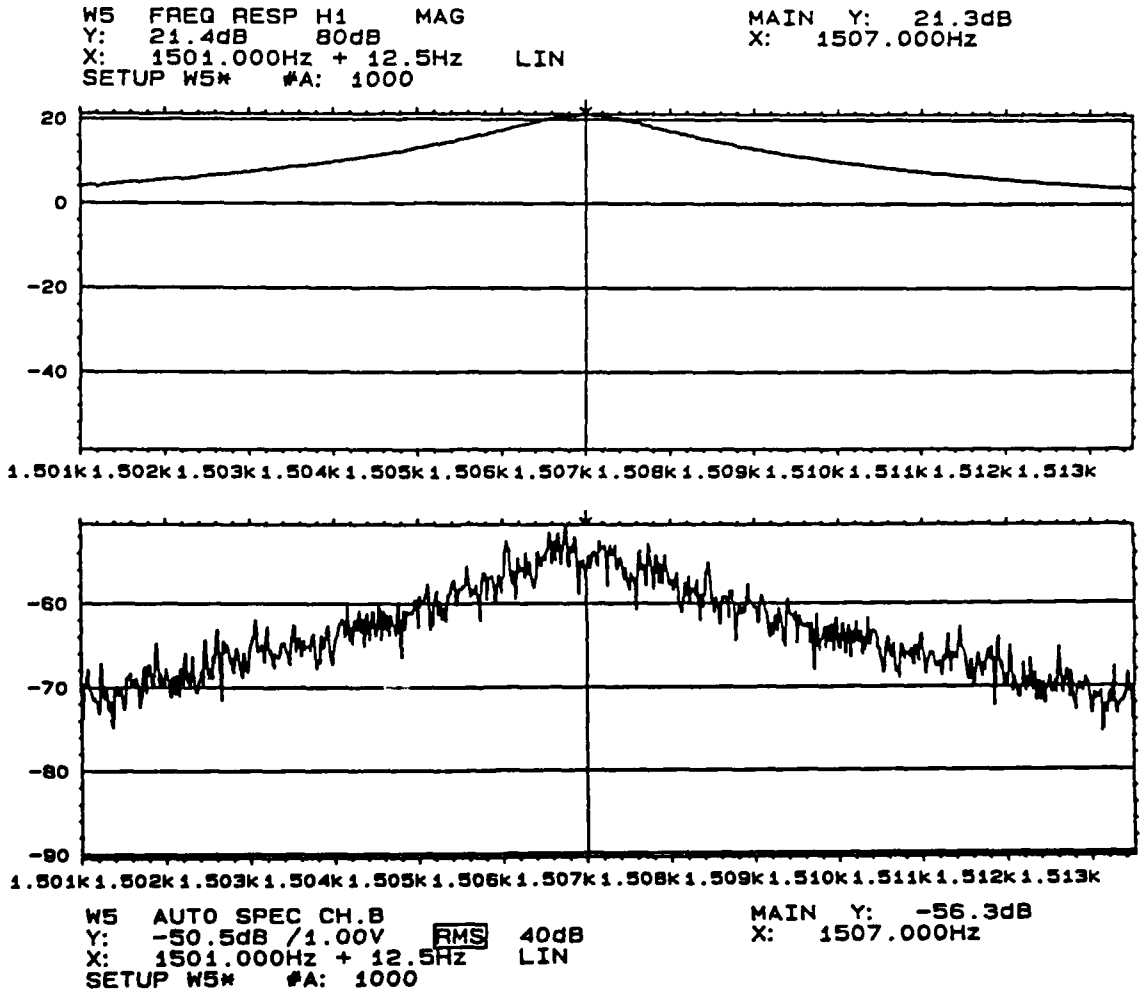

Figure 4.1 FFT of mode 1 for 7% Gr(p-r)/Al

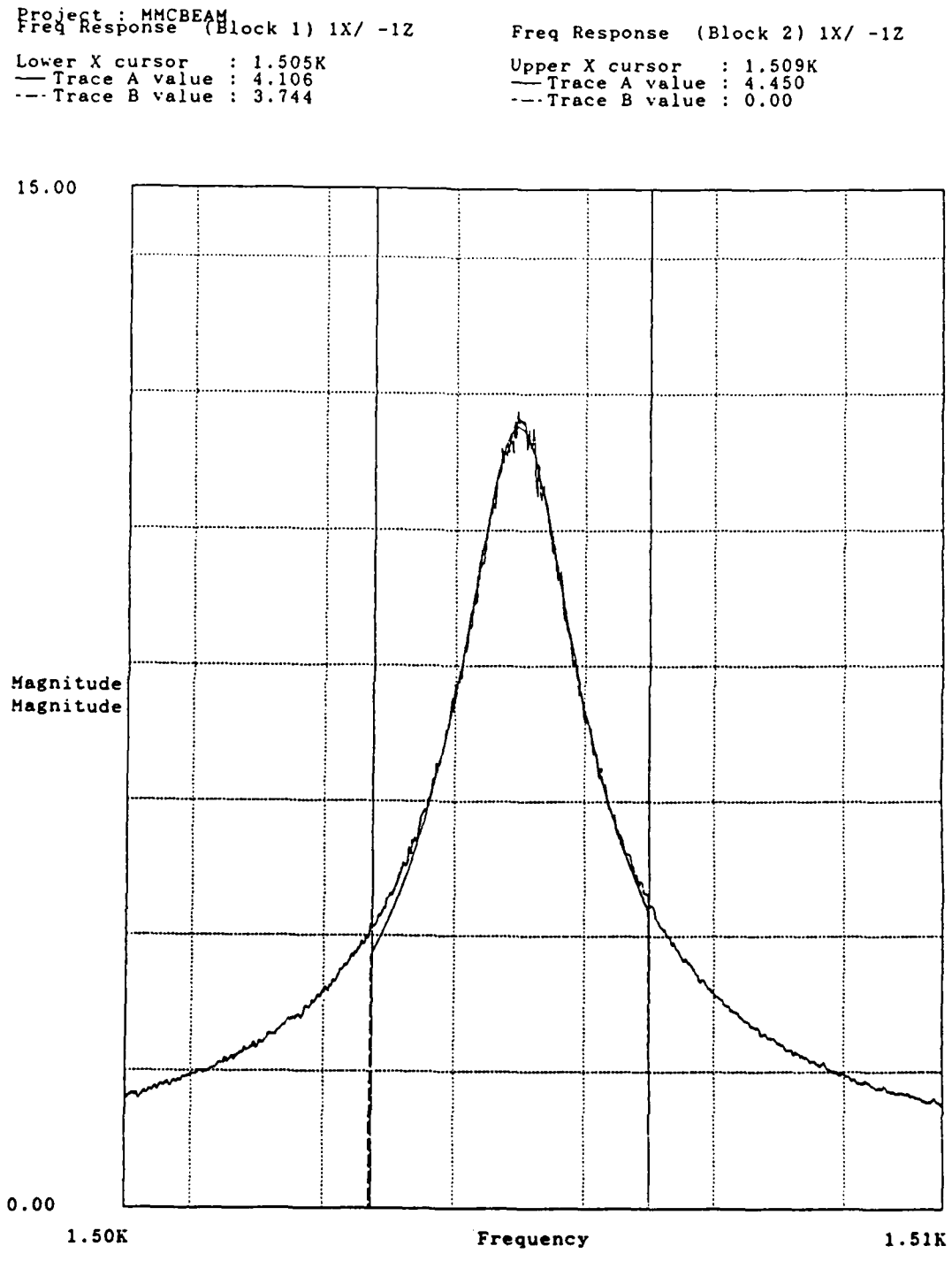

Figure 4.2 Curve fit of mode 1 data for 7% Gr(p-r)/Al

ensure that theoretically calculated node points were valid. This was accomplished by moving the pickup point of the vibrometer along the length of the beam. The time channel of the input signal from the generator was traced out against the time channel of the output signal from the vibrometer forming a Lissajous loop. The Lissajous loop became flat on a node since the velocity of a node point was negligible. Additionally, the slope of the Lissajous loop changed sign when the laser pickup point passed from one side of a node to the other. This was due to the phase shift of 180 degrees which occurs between the generator signal and the velocity signal on different sides of a node. Using this technique, the nodes of the anisotropic materials were found to be in agreement with the theoretical values to within the error of the nodal position determination technique. Viscous losses were calculated to be on the order of 10^{-6} which would not significantly effect the experimentally measured damping. Viscous losses were small due to the low velocity of vibration of the specimen (on the order of 10^{-4} m/sec or less). Air damping occurs when the specimen radiates acoustic energy into the environment. Coincidence frequency for a plate is defined by the following equation [28]:

$$f_c = \frac{\sqrt{3}c_o^2}{\pi h}\sqrt{\frac{(1-\nu^2)\rho}{E}} \qquad (4.1)$$

For a beam specimen, the $(1-\nu^2)$ factor is ignored. Below the coincidence frequency the specimen radiates negligible energy into the environment. Above the coincidence frequency, the specimen is an efficient radiator and significant air damping can result. This effect is often ignored by researchers. It is also a difficult effect to

quantify. Approaching the problem through the use of acoustical radiation theory results in integrals which are very difficult to solve. Beams present an even more intractable problem than plates [29]. This means that exact solutions are not possible and the equations must be solved by the use of approximations which limit application to frequencies either well above coincidence or well below it [28,30,31]. Unfortunately, the frequency range used in this investigation does not lend itself to the application of these solutions since coincidence occurs practically at the center of the frequency range. From this it must be concluded that the theoretical determination of air damping as a function of material, specimen geometry and frequency is unlikely. The best way to avoid air damping is to either make all measurements below coincidence or to make measurements in a vacuum chamber. A vacuum chamber was not available for this investigation. Therefore all damping measurements made above coincidence could contain substantial air damping and must be analyzed with this in mind. Zener [4] has stated that the use of a vacuum chamber was necessary when the loss factor was less than 10^{-4}. Since the lowest loss factor which was measured was about $.8 \times 10^{-4}$ (mode 1 of steel), it is apparent that the measurement technique is at the threshold where a vacuum chamber is required. Hence, low damping materials will be more strongly affected than high damping materials since radiation losses will represent a larger proportion of their measured loss factors.

Torsional modes were encountered in the measurements. Torsional modes present problems when they occur in the vicinity of the transverse modes of interest. It was difficult to isolate which modes were

transverse and which modes were torsional by the use of predicted mode frequencies. This was because the actual frequencies of the two different types of modes could lie within the error of their predicted frequencies. Two such modes are pictured in Figures 4.3 and 4.4. In Figure 4.3, the pickup point of the laser was on the corner of the beam. In Figure 4.4, the pickup point was moved to the center of the beam. Since the torsional modes have a node running up the center of beam, a corresponding decrease in a torsional mode should occur when the pickup point is moved to towards the midline of the beam. The higher frequency mode drops relative to the lower frequency mode as shown in Figure 4.3 and 4.4 and must therefore be the torsional mode.

The damping of 6061-T6 Al and a plain carbon steel are plotted in Figure 4.5. Here it is seen that for both steel and aluminum, the damping decreases from the mode 1 to mode 2 and then increases from mode 2 on up to mode 4. At mode 4, steel peaks and then falls to a lower value at mode 5 while aluminum continues to rise at mode 5. It so happens that coincidence occurs just below mode 2 for both steel and aluminum. Table 4.1 lists the specimen geometries and coincidence frequencies for all the damping specimens which were tested. In light of the fact that the measured damping begins to increase precisely above the coincidence frequency, it is apparent that air damping is not negligible above the coincidence frequency. It is possible that the shape of the curves in Figure 4.5 is caused to some degree by the superposition of two relaxation mechanisms. If this is indeed the case, then the two most likely mechanisms are the relaxation of transverse thermal currents and the relaxation of intercrystalline thermal

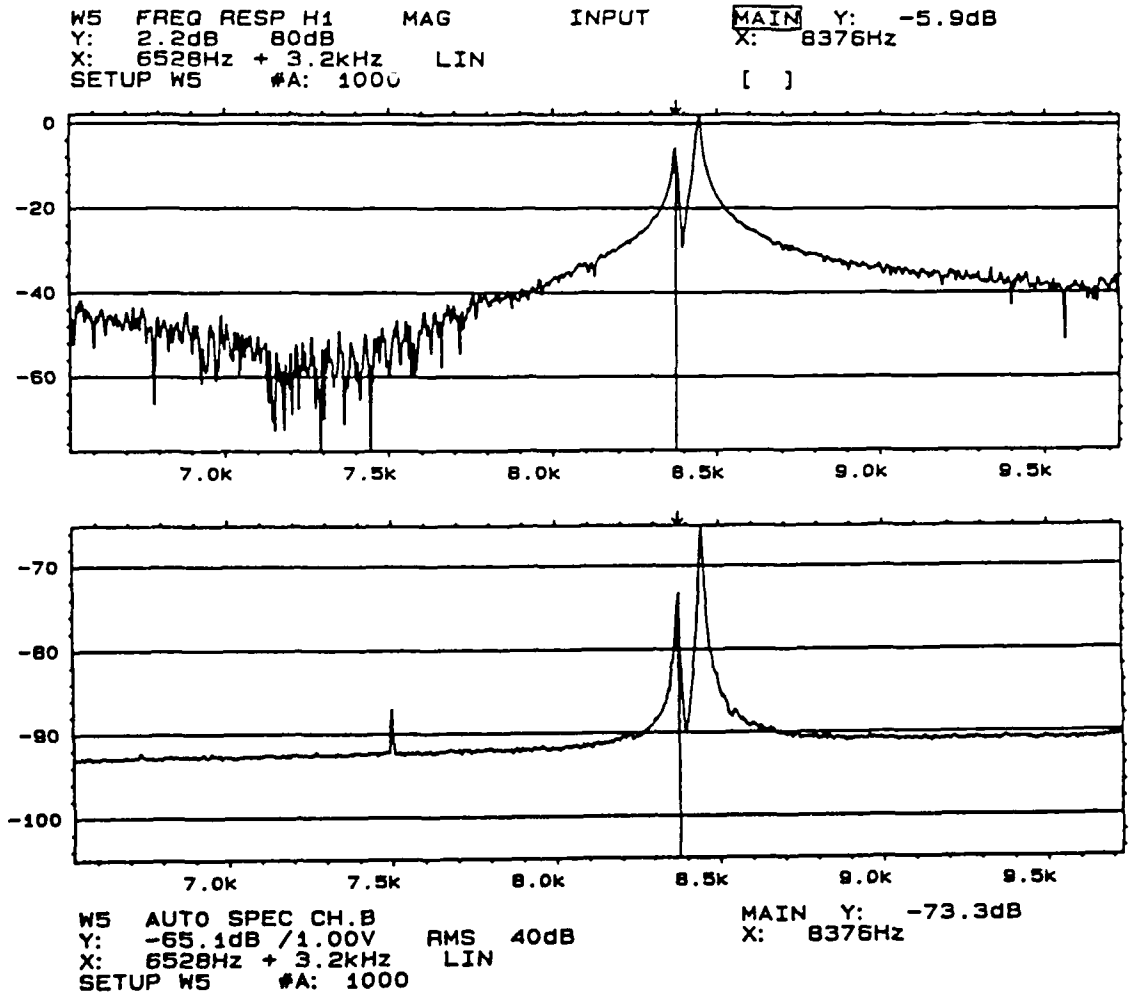

Figure 4.3 FFT of detection on the corner of the beam

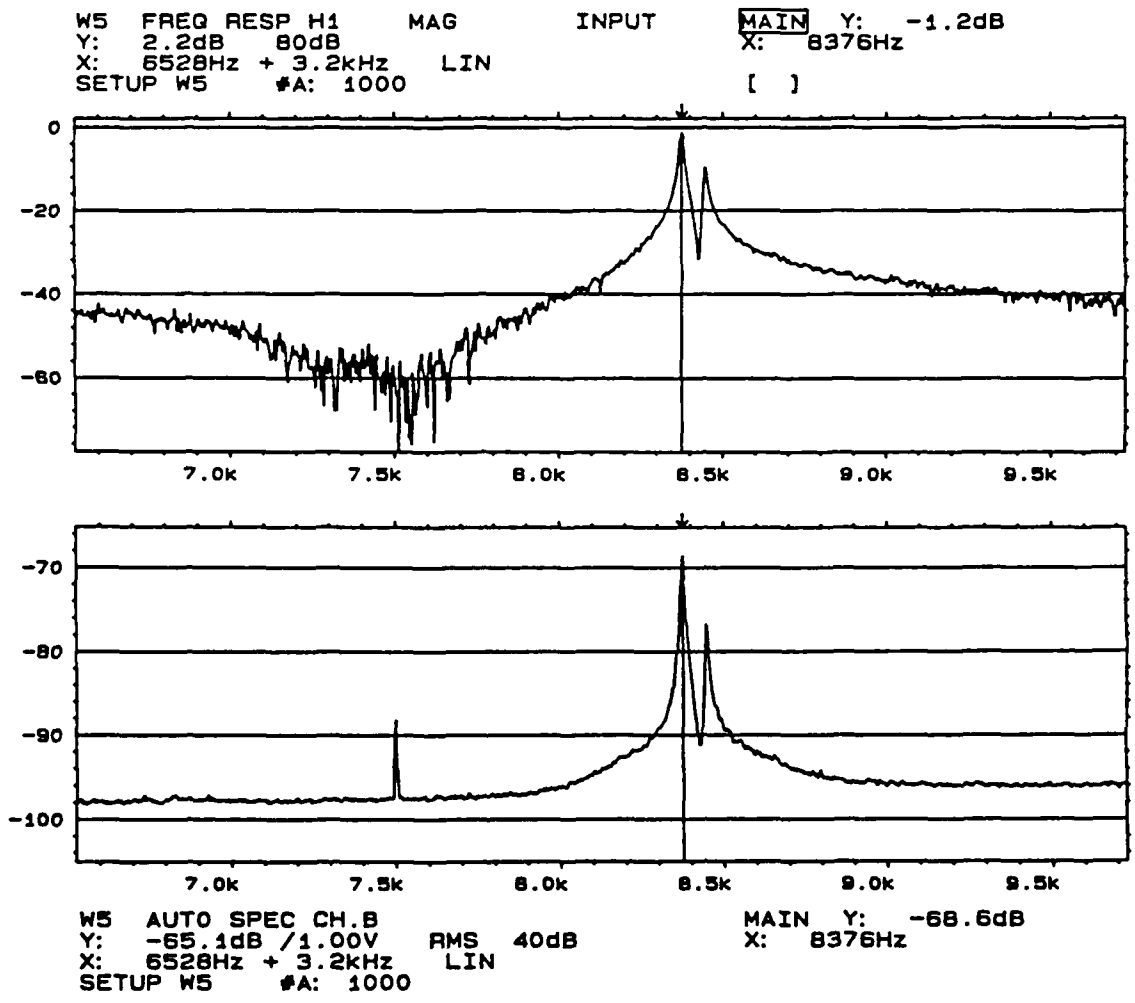

Figure 4.4 FFT of detection on the center of the beam

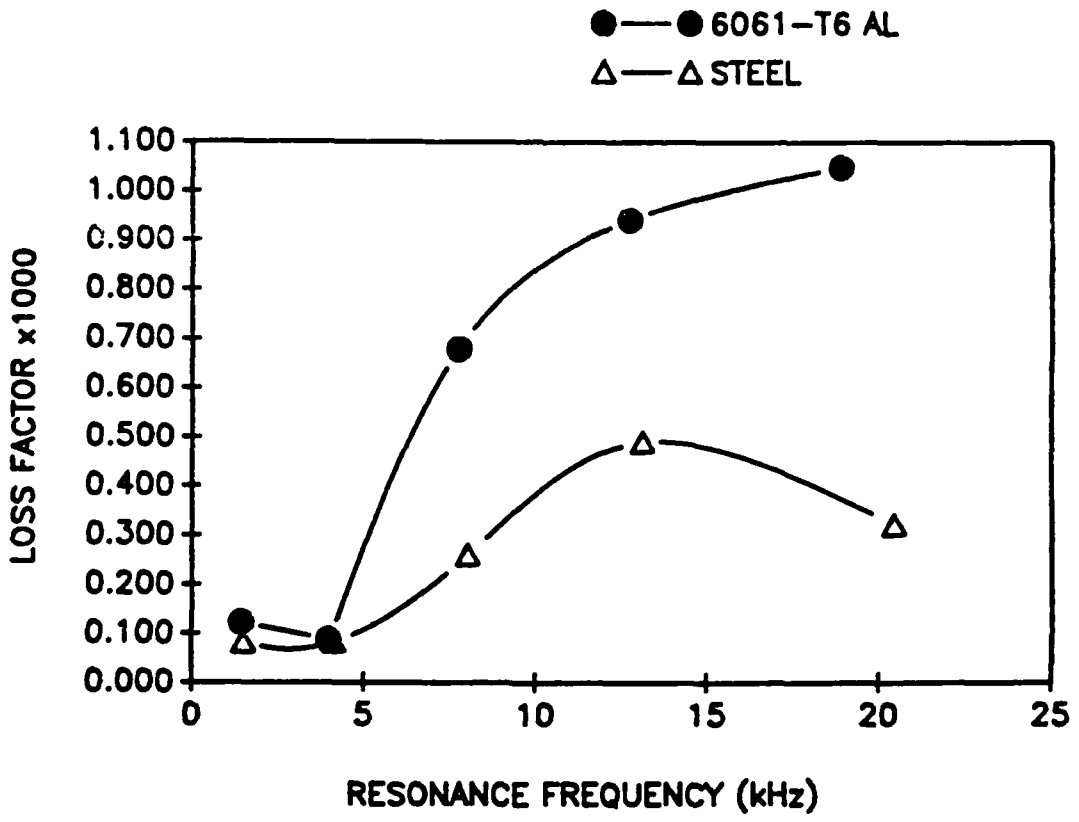

Figure 4.5 Plots of the loss factors for wrought 6061-T6 Al and a plain low carbon steel (the data points correspond to modes 1 through 5 for both materials)

Table 4.1 Specimen Geometries and Coincidence Frequencies

SPECIMEN:	LengthxWidthxHeight: (mmxmmxmm)	Coincidence Frequency: (Hz)
6061-T6 Al	100x9.93x2.79	4630
Steel	101x12.7x2.95	4280
Al-Mg (MA)	85.4x8.30x1.35	9120
SiC_p/Al (MA)	108x5.59x1.28	8350
SiC_p/Al	95.2x5.08x1.19	9760
Al_2O_3(p)/Al	100x9.93x2.82	3670
SiC_w/Al	100x9.88x2.74	3280
SiC/Al	101x7.59x1.68	6790
Gr/Al	101x7.62x1.65	5500
0% Al	102x9.66x3.35	3840
7% Gr(p-r)/Al	104x12.7x3.35	3650
15% Gr(p-r)/Al	104x12.7x3.15	3680
27% Gr(p-r)/Al	104x12.8x3.10	3530
Nitinol	101x10.1x2.82	7230
Incramute	100x9.90x2.82	6450

currents. These relaxations are described by Zener [4] and Norwick and Berry [2]. The transverse thermal current relaxation has been experimentally verified by Zener [4], Berry [32], and Wren and Kinra [33]. The relaxation of intercrystalline thermal currents has been experimentally verified by Randall et al. [34], Entwistle [35] and Kerlin [36]. The relaxation time for transverse thermal currents is given by:

$$\tau=\frac{h^2\rho C_P}{\pi^2 k_t} \tag{4.2}$$

The relaxation strength for transverse thermal currents is given by:

$$\eta_o=\frac{\alpha^2 ET}{\rho C_P} \tag{4.3}$$

For the 6061-T6 Al specimen, the transverse relaxation time and strength are $11.46\text{x}10^{-3}$ seconds and $4.64\text{x}10^{-3}$, respectively (see Appendix A). The transverse thermal current relaxation reaches its maximum at about 10 Hz. However, since 6061-T6 Al has a relatively large relaxation strength, it could still contribute to the low measured damping of mode 1 and possibly mode 2. Figure 4.6 shows a plot of the calculated transverse thermal current damping. This represents 35% of the measured mode 1 value and 19% of the mode 2 value, assuming that the theory exactly predicts the contribution of the thermal current relaxation to the damping. Other damping mechanisms, support losses and air damping also account for damping measured above the predicted transverse thermal current damping.

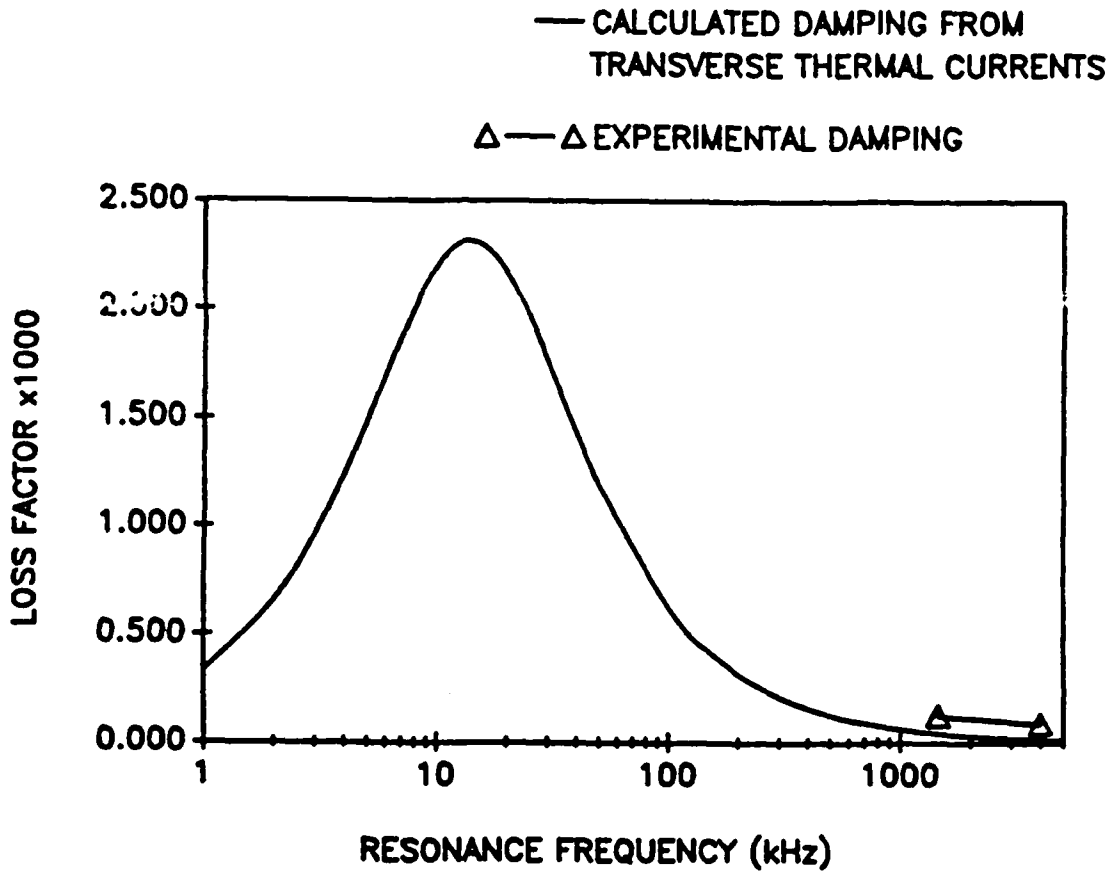

Figure 4.6 Plot of the calculated transverse thermal current damping and actual experimentally measured damping for wrought 6061-T6 Al

The intercrystalline thermal current relaxation has a time constant given by:

$$\tau=\frac{d^2\rho C_P}{3\pi^2 k_t} \tag{4.4}$$

and a strength which is estimated by:

$$\eta_o=\frac{R(3\alpha)^2 T k_t}{C_P} \tag{4.5}$$

Experimental work [34] suggests that the actual relaxation strength is about an order of magnitude less than that given by equation 4.5. The value for the aluminum specimen which is calculated from equation 4.5 is unreasonably large compared to the measured maximum value from Figure 4.5. Therefore, no accurate estimate of the relaxation strength is available since a good estimation must be approximately equal to or less than twice the maximum measured damping i.e. $\eta_{meas} \leq \frac{1}{2}\eta_o$. The grain size of the wrought 6061-T6 Al specimen was determined to be on the order of 0.12 mm. The maximum damping associated with the intercrystalline thermal current relaxation is then calculated to occur around 22.6 kHz. This agrees well with Figure 4.5 in which aluminum appears to be reaching its maximum damping in the 22.6 kHz vicinity. However, in Figure 4.5, the curve does not resemble a typical superposition of two relaxations. Figure 4.7 was generated by plotting the following equation (see Appendix B):

$$\eta_{o_{TOTAL}}=\eta_{o_{TTC}}\frac{\omega\tau_{TTC}}{1+(\omega\tau_{TTC})^2}+\eta_{o_{ICTC}}\frac{\omega\tau_{ICTC}}{1+(\omega\tau_{ICTC})^2} \tag{4.6}$$

This equation represents the superposition of the two relaxations. The relaxation strength, η_{oICTC}, has been calculated so that equation (4.6)

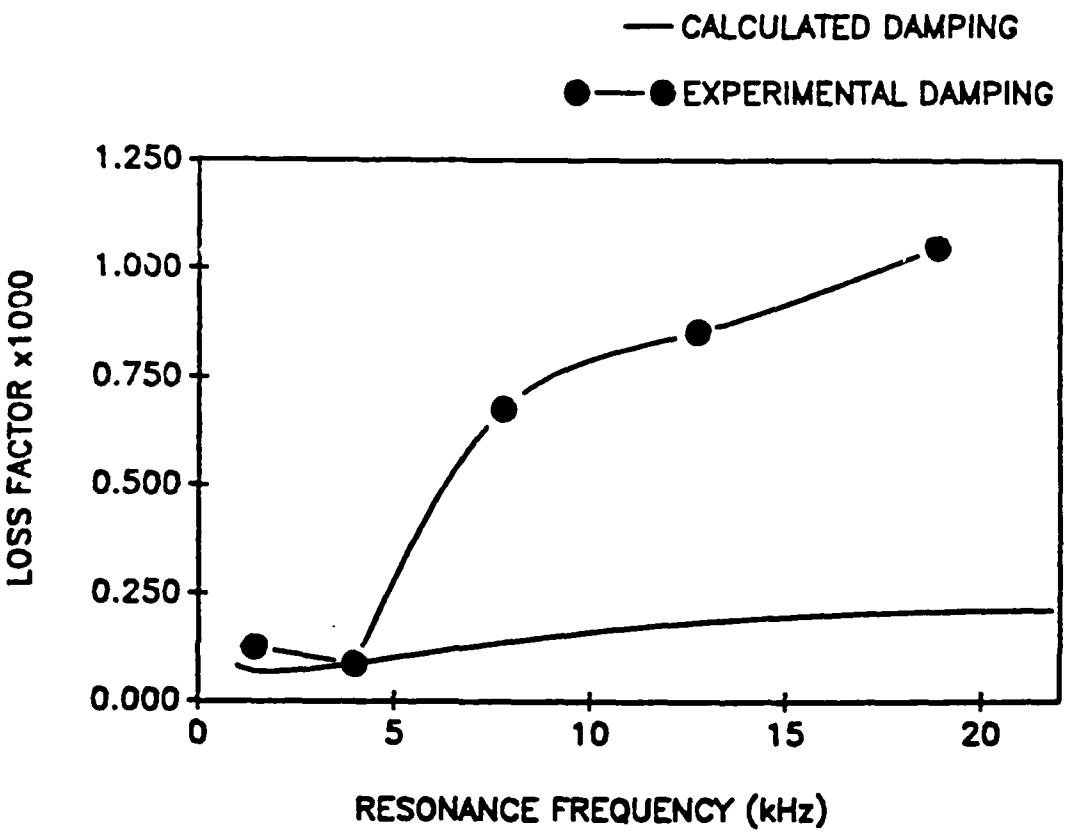

Figure 4.7 Plots of experimentally measured damping and theoretically calculated damping assuming a superposition of two relaxations for wrought 6061-T6 Al

does not exceed any of the measured values. The measured damping of mode 2 was the limiting value and thus equation (4.6) was calculated so that η_{total} equalled the measured value at mode 2 as can be seen in Figure 4.7. It is apparent from Figure 4.7 that intercrystalline thermal currents are responsible for only a marginal increase in the measured damping above coincidence. Figure 4.5 shows that steel exhibits a maximum well above its coincidence frequency. This seems to indicate that perhaps there is some mechanism which is causing a damping maximum since air damping would be expected to increase with increasing frequency. However, acoustic radiation theory indicates that at some point above the coincidence frequency, the radiation resistance becomes a constant value given by [31]:

$$R_r=\rho c(2WL) \tag{4.7}$$

Loss factor is related to radiation resistance by:

$$\eta_R=\frac{R_r}{M\omega} \tag{4.8}$$

Therefore, at some point above the coincidence frequency, the loss factor has an inverse frequency dependence. Unfortunately, their is no theoretical way to estimate when the high frequency limit becomes valid. For this reason, the applicability of equation (4.8) is addressed in an unrigorous manner in Appendix C. Figure 4.8 is the result of the subtraction of the damping predicted from equations (4.7) and (4.8) from the measured values for the modes 4 and 5 for steel, along with measured values for mode 1 and 2. Recall that the air damping below coincidence has been determined to be negligible and has been ignored. Mode 3 has

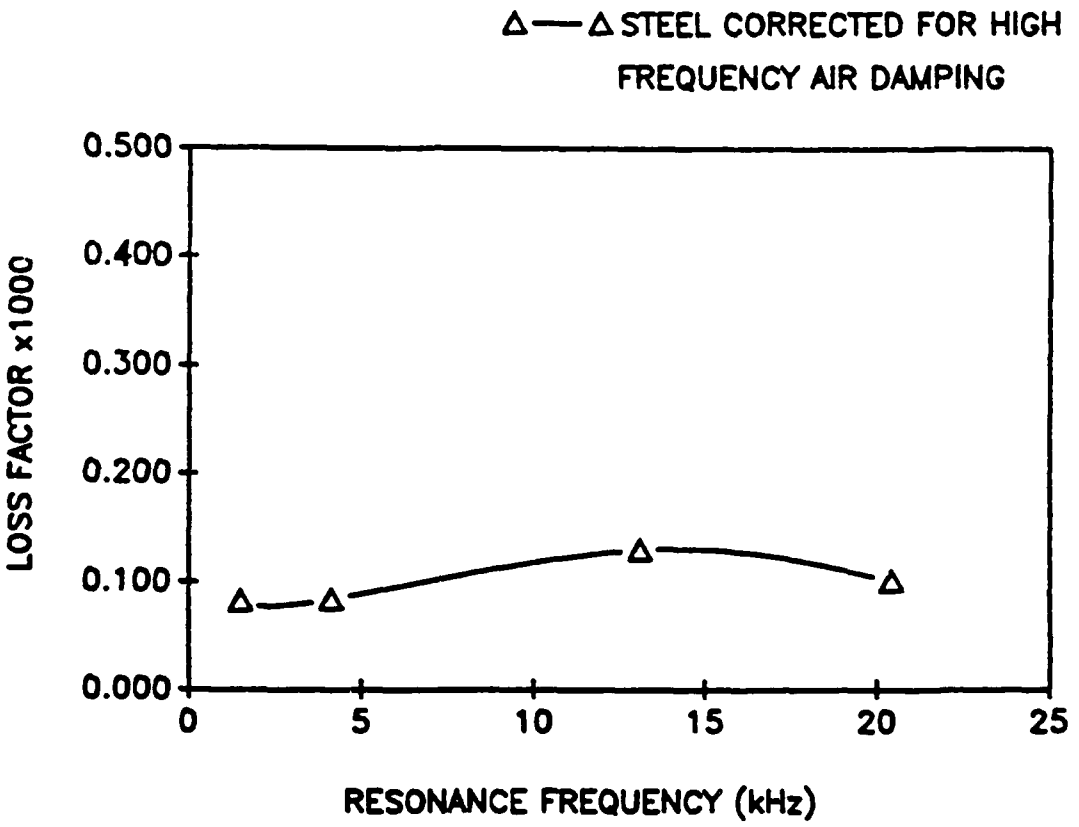

Figure 4.8 Plot of experimental damping data for plain low carbon steel after modes 4 and 5 have been corrected for high frequency limit air damping (mode 3 has been excluded since the high frequency limit was apparently not valid for this mode)

not been included in this figure since it represents a transition regime for which the theoretical prediction of air damping is intractable. This figure reveals that the damping of steel is essentially frequency independent after high frequency air damping has been subtracted. It can therefore be concluded that the effects of intercrystalline thermal currents are at most minimal. Further, the measurement of η above the coincidence frequency does not accurately reflect the nature of the damping in steel. The same is perhaps true for aluminum as well. However, it is still possible that specimens with higher structural damping will provide meaningful results since air damping will represent a smaller proportion of the measured damping. Conclusions must be drawn on a case by case basis. It is also important to realize that despite the difficulties of interpreting the post-coincidence damping data, the pre-coincidence damping data are still essentially unaffected by air damping. The main source of error below coincidence is support losses which are likely to be much less than post-coincidence radiation losses. Further, the support losses will depend less on specimen geometry and material than will post coincidence air damping. The topic of support losses will addressed further in section 4.2.1.

4.2 Improved Damping by the Intrinsic Approach

4.2.1 Mechanically Alloyed Materials

The mechanical properties of all of the materials studied in this investigation are presented in Table 4.2. It can be seen that the mechanically alloyed Al-Mg material has significantly higher UTS than 6061-T6 Al and a modulus slightly higher than 6061-T6 Al. The mechanically alloyed SiC_p/Al-Cu composite also has good strength and stiffness in relation to 6061-T6 Al. The damping of these materials is shown in Figure 4.9. It is seen that the two mechanically alloyed materials do not show the rapid increase in damping that aluminum or even steel exhibited. This is because coincidence for the mechanically alloyed specimens is nearly twice that of the aluminum. Coincidence is at a higher frequency for the mechanically alloyed materials because the mechanically alloyed specimens are thinner than the aluminum and the steel (see Table 4.1). The mechanically alloyed materials show unusually high damping down towards the first mode. These materials have about three times the damping of aluminum for the first mode. This damping is primarily due to transverse thermal current relaxation. Even though the relaxation strength of the mechanically alloyed materials is approximately that of the aluminum, the relaxation time of the mechanically alloyed specimens is less than one-fourth of aluminum. This means that the frequency of maximum damping for the mechanically alloyed materials is more than four times that of the aluminum. This effect is caused by the smaller thickness of the mechanically alloyed

Table 4.2 Mechanical Properties of the Materials

SPECIMEN:	YOUNG'S MODULUS: (GPa)	UTS: (MPa)
6061-T6 Al	69	310
Steel	207	725
Al-Mg (MA)	75	448
SiC_p/Al (MA)	103	620
SiC_p/Al	90	382
Al_2O_3(p)/Al	114	271
SiC_w/Al	148	577
SiC/Al	101	276
Gr/Al	130	175
0% Al	69	140
7% Gr(p-r)/Al	75	193
15% Gr(p-r)/Al	81	252
27% Gr(p-r)/Al	87.3	322
Nitinol	66	
Incramute	96.5	537

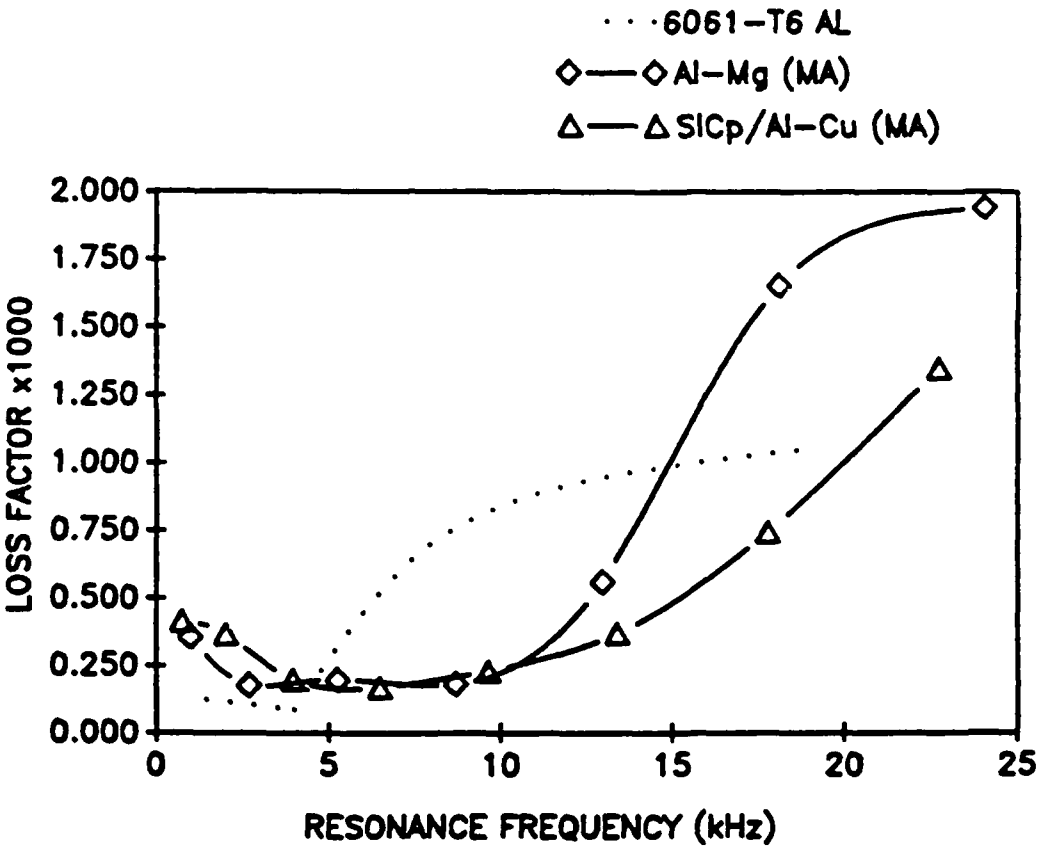

Figure 4.9 Plots of the loss factor of the mechanically alloyed materials [Al-Mg (MA), SiC_p/Al-Cu (MA)] and wrought 6061-T6 Al

specimens. The calculated transverse thermal current damping for the Al-Mg (MA) specimen represents 84% of the measured mode 1 value and 66% of the measured mode 2 data. At the higher frequencies where transverse thermal current relaxation becomes less significant, it is seen that the mechanically alloyed materials appear to have only marginally better damping than the pre-coincidence damping of the aluminum. The flatness and similarity of the damping data of the mechanically alloyed materials as they approach coincidence is further confirmation that radiation losses are primarily responsible for the post-coincidence damping of the aluminum.

The fact that the mode 1 data for the Al-Mg (MA) specimen was due largely in part to the relaxation of transverse thermal currents yields insight into the sources of extraneous damping for the experimental technique. Since 84% of the damping was due to relaxation, 16% , or 5.8×10^{-5} of the measured loss factor of 3.6×10^{-4} must be representative of the extraneous losses due primarily to support losses and possibly some pre-coincidence radiation losses. This value can be compared against the calculated mode 1 support losses of the aluminum specimen. The aluminum specimen had a measured mode 1 loss factor of 1.26×10^{-4} of which 35% was due to transverse thermal current relaxation. The damping of the aluminum specimen resulting from deviation from relaxation theory, other mechanisms of damping, support losses and radiation losses corresponds to 65% of 1.26×10^{-4} which is 8.2×10^{-5}. This is in reasonable agreement with the calculated losses unaccounted for by relaxation of thermal currents for the Al-Mg (MA) specimen. The difference could be due to the dependence of extraneous losses on

specimen geometry and material. The calculated support losses are also a conservative estimate since other damping mechanisms could be part of the measured mode 1 damping values.

4.2.2 Particulate MMCs

The mechanical properties of the particulate composites as listed in Table 4.2 show that these MMCs all have superior stiffness and strength compared with 6061-T6 Al (except for the $Al_2O_3(p)$/Al which has lower strength than 6061-T6 Al). The damping of the three particulate composites is shown in Figure 4.10 along with the reference data for aluminum. Plots in Figure 4.10 look very similar to those in Figure 4.9 in many respects. The damping of the SiC_p/6061 Al composite looks very similar to the damping of the Al-Mg (MA) material, except that the composite has almost twice the damping for mode 1. This effect is again due to transverse thermal current relaxation. The SiC_p/6061 Al specimen is thinner than the Al-Mg (MA) specimen. This not only lowers the damping maximum for the relaxation but also lowers the resonance frequency of the beam. Hence, the combined effect causes the lower modes of thin specimens to have higher damping. The $Al_2O_3(p)$/Al resembles the aluminum specimen since they both have the same dimensions. In general however, the damping of the particulate composites, neglecting the geometrical differences, is no better than that of the aluminum.

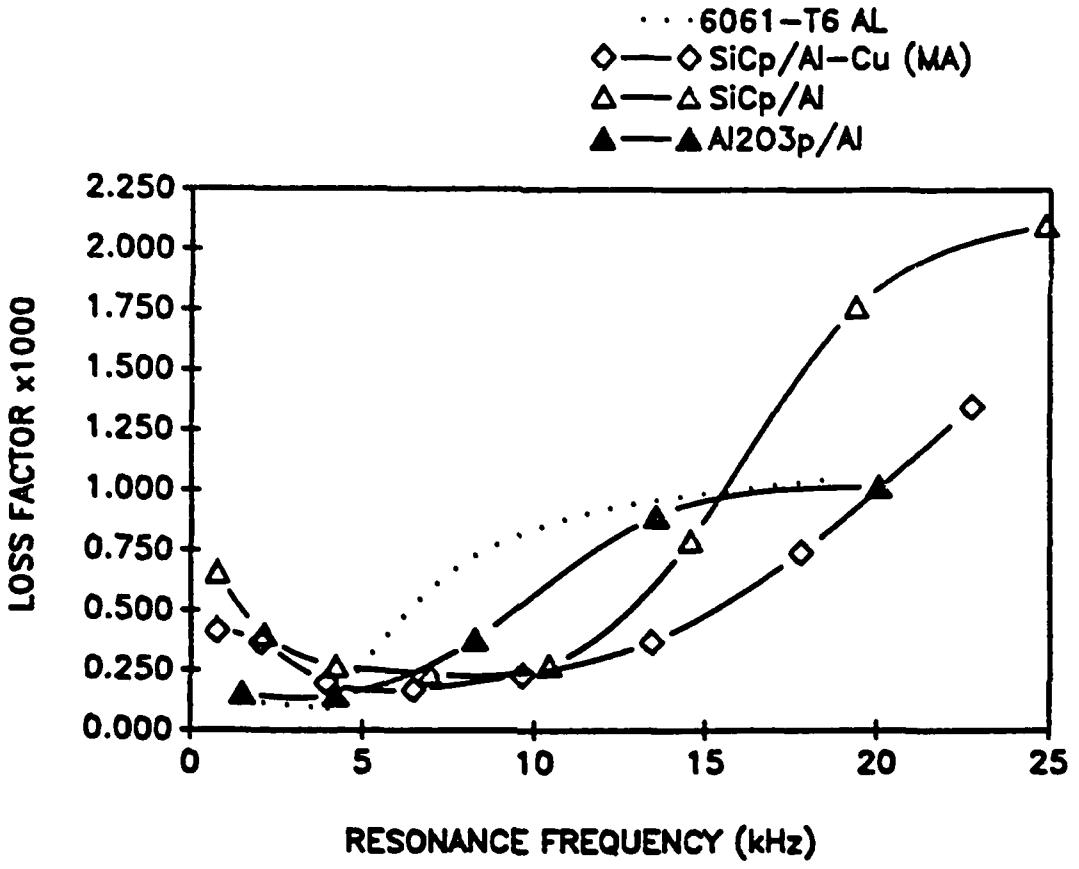

Figure 4.10 Plots of the loss factor of the particulate reinforced composites [SiC_p/Al-Cu, SiC_p/6061 Al, Al_2O_3(p)/Al] and wrought 6061-T6 Al

4.2.3 Whisker MMCs

The SiC_W/Al composite has very attractive mechanical properties. It has twice the modulus of aluminum and nearly three times the tensile strength of 6061-T6 Al. The damping of SiC_W/Al is shown in Figure 4.11 along with reference data for the aluminum specimen. The damping of SiC_W/Al is almost identical to that of the aluminum. It is apparent that the SiC_W/Al offers no improvement in damping over aluminum.

4.2.4 Continuous Fiber MMCs

The tensile test results for unidirectional Gr/Al and SiC/Al are in Table 4.2. These composites were made by the HiPIC technique described earlier. Unidirectional fiber reinforced SiC/Al composites fabricated by this technique are shown in Figure 4.12 to have an overall uniform fiber distribution. Figure 4.13 shows that the individual filaments of the fiber tows are surrounded by the matrix material indicative of good infiltration. Figure 4.14 shows the fracture surface of a HiPIC composite. Fiber pullout is predominant which indicates a weak interface. In Figure 4.15, higher magnification of the pulled out fibers reveals that they are relatively devoid of reaction products.

Enhanced damping of continuous P55 Gr/6061 Al has also been reported by Rawal and Misra [11]. They observed strain amplitude dependent damping for both 6061 Al and for the composites. The composites exhibited as much as three times the damping of the aluminum. However, the damping was generally less depending on strain amplitude,

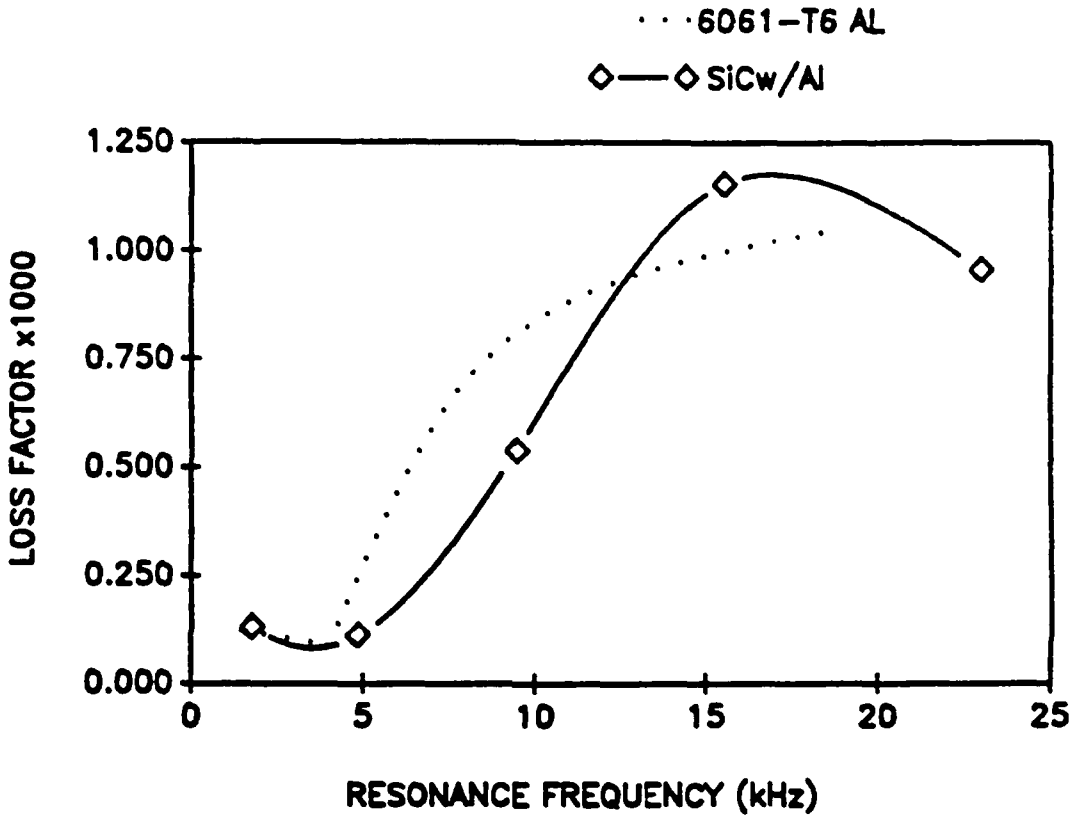

Figure 4.11 Plots of the loss factor of the whisker reinforced composite [SiC_w/Al] and wrought 6061-T6 Al

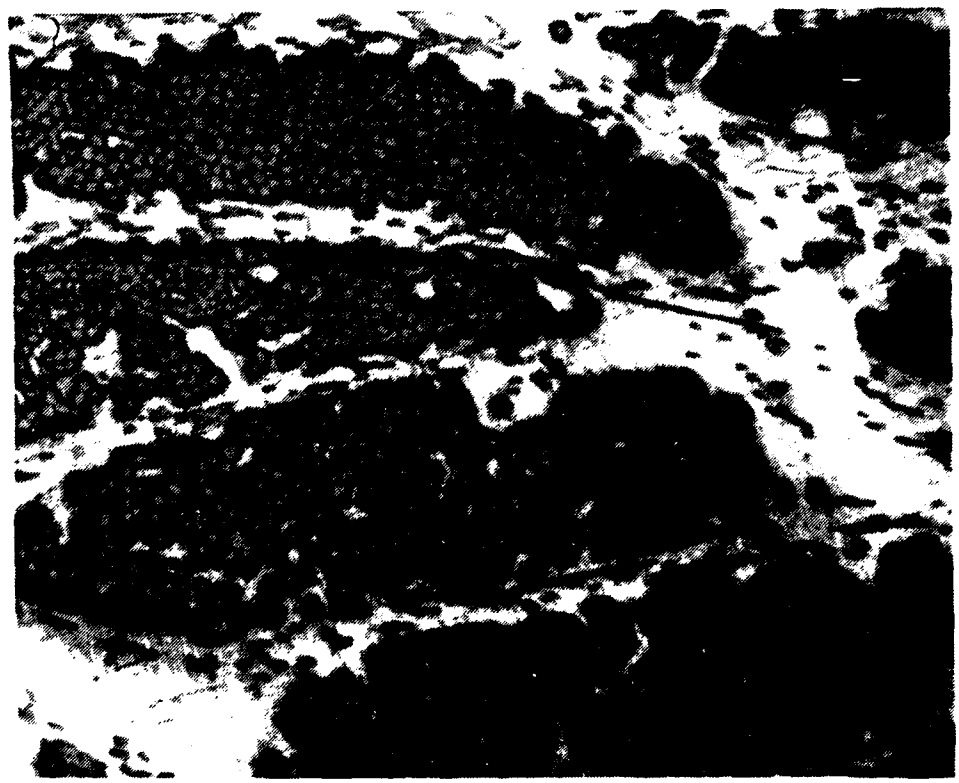

Figure 4.12 Micrograph showing the overall fiber distribution in a unidirectional SiC/Al composite (X100)

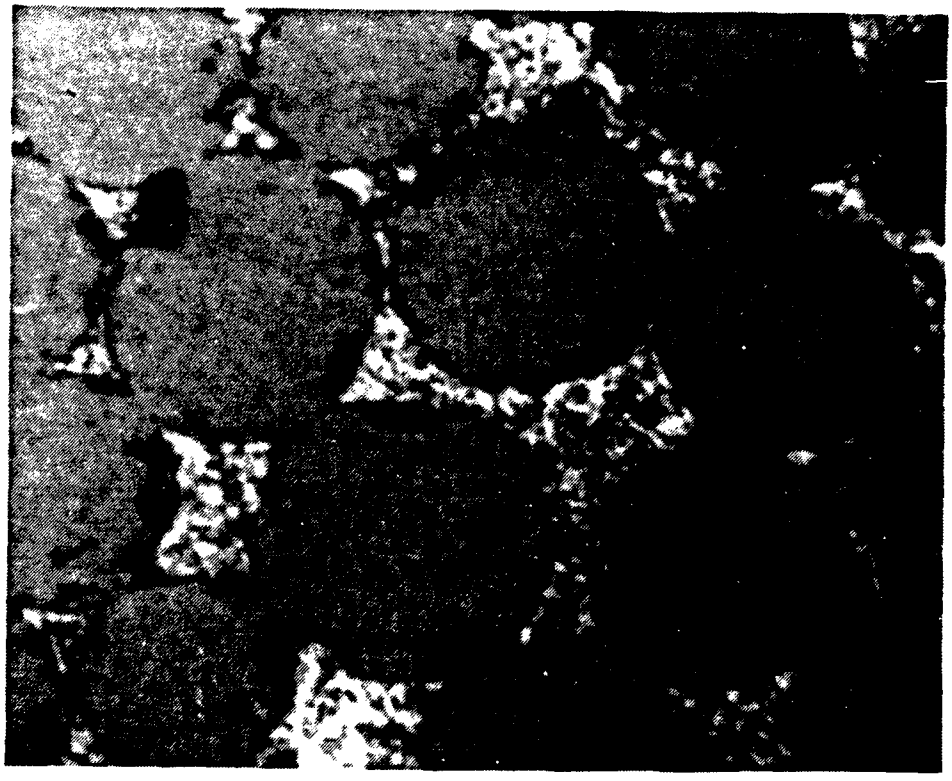

Figure 4.13 Micrograph showing the thorough infiltrat[illegible] of a fiber tow in a unidirectional SiC/Al composite (X2000)

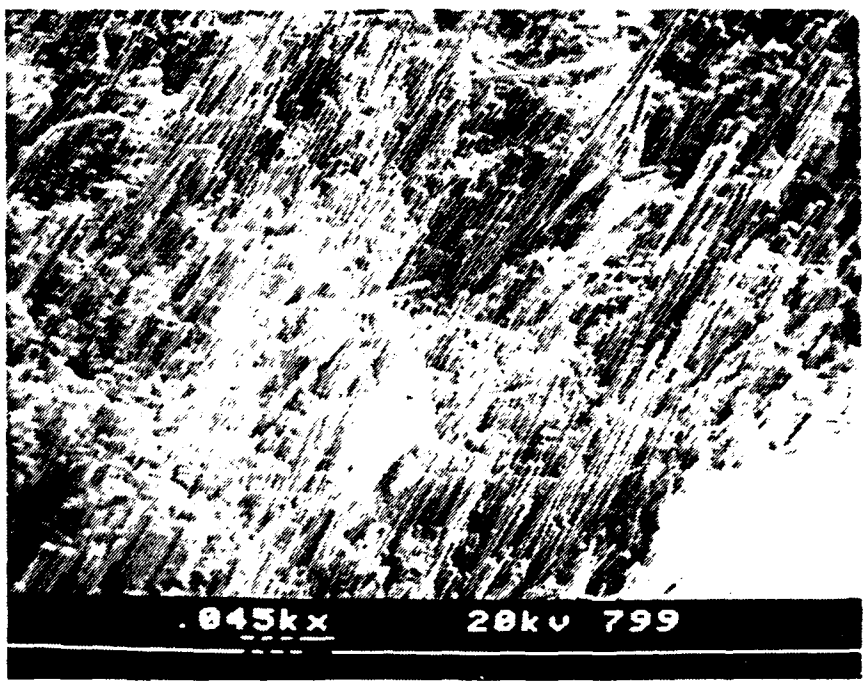

Figure 4.14 Micrograph showing fiber pullout at a fracture surface in a unidirectional SiC/Al composite

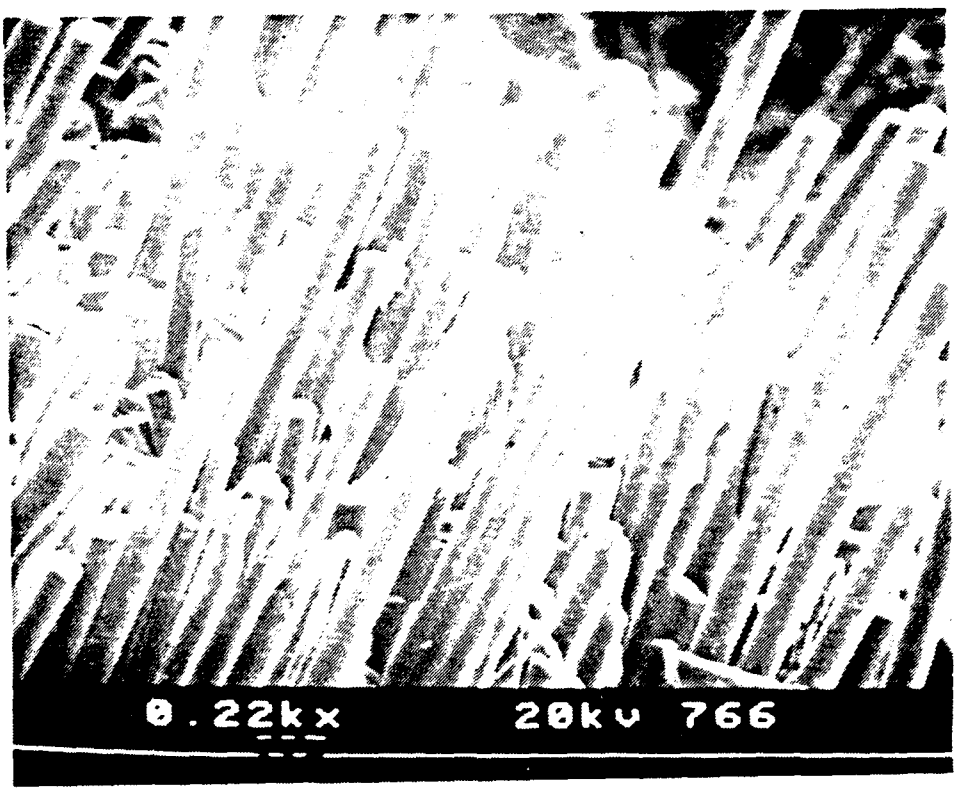

Figure 4.15 Micrograph showing fibers protruding from the fracture surface of a unidirectional SiC/Al composite

fiber orientation and consolidation parameters. Wren and Kinra [37] reported values for P55 Gr/6061 Al composites which were lower than their annealed 6061 standard. They observed a weak strain amplitude dependence. Wren and Kinra reported damping values for P55 Gr/Al which were about 3 times less than those of Rawal and Misra. This is based on data for strain amplitudes of $30x10^{-6}$. Even though one investigation measured damping of composites to be greater than an aluminum standard and the another investigation measured the opposite, both investigations reported nearly the same value for the aluminum standard.

The damping of the unidirectional Gr/Al and SiC/Al composites is shown in Figure 4.16. It is evident that the damping of these two composite specimens is very similar. More importantly, Figure 4.16 shows the first evidence of significantly improved damping of MMCs over the aluminum specimen. A comparison of mode 2 data shows that Gr/Al has about 4.1 times the damping of the aluminum. Similarly, SiC/Al has about 5.2 times the damping of the aluminum. Mode 2 is selected for this comparison because, for aluminum, it is still a pre-coincidence data point and has less transverse thermal current relaxation damping in it than the mode 1. The damping of unidirectional composites in the transverse direction is generally several times greater than the damping in longitudinal direction. Wren and Kinra [13] used general laminate theory to predict the damping of laminated composites as a function of angle. They obtained reasonable agreement between experiment and theory. They measured the damping in the transverse direction to being about 4 times that of the longitudinal direction. In the present investigation, the transverse direction was found to have 5.1

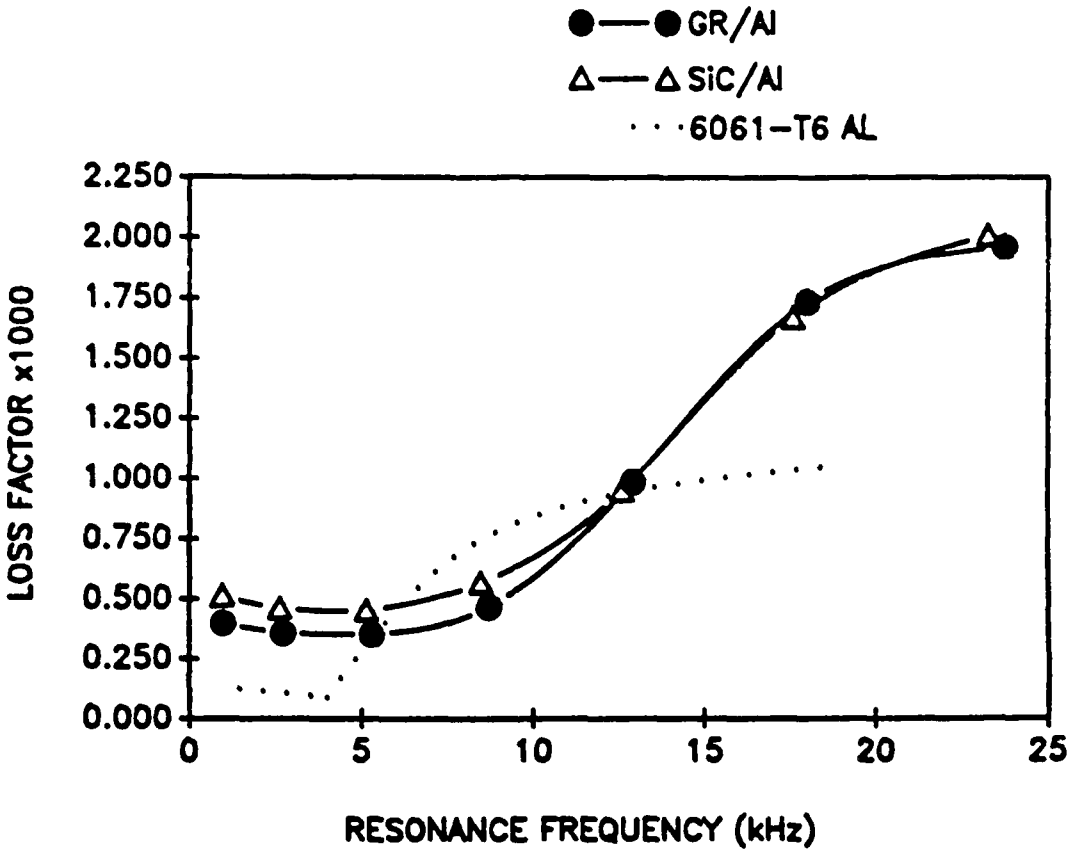

Figure 4.16 Plots of the loss factor of the unidirectional composites [Gr/Al, SiC/Al] and the wrought 6061-T6 Al

(η_T =.00198) times the damping of the longitudinal orientation for the unidirectional Gr/Al and about 2.8 (η_T =.00141) times for the unidirectional SiC/Al. The following explanation will show that the damping of the composites is not due to transverse thermal current relaxation. For example, the relaxation contributes about $5x10^{-5}$ to mode 2 damping for Gr/Al. This represents only about 13% of the measured value. This also holds for the SiC/Al. One important observation is that the continuity of the fibers may play an important role. It appears that it is not sufficient that the reinforcement is simply contained in the matrix. If this were true, then the SiC_p/Al composite would show similar damping because it contains roughly the same amount of SiC as the unidirectional SiC/Al but in a different spacial arrangement. This could be significant because if the reinforcement is shorter than a critical length, then the shear stresses at the interfaces have only a limited amount of surface area with which load can be transferred to the reinforcement. This means that residual stresses in continuous fiber composites will be larger than composites with reinforcements shorter than the load transfer length. Additionally, relatively lower stress levels will be reached in the composites with reinforcements which are smaller than the load transfer length. Therefore, continuous fiber composites will have larger residual stresses and higher interfacial stresses. This could enhance some form of dislocation relaxation or resonance. However, it is questionable as to whether or not a dislocation mechanism would be responsible for damping measured in the kHz range at room temperature [6] because room temperature dislocation damping peaks in composites

generally occur in the MHz range. Interfacial friction is another possible mechanism. Even though the strain amplitude of the test is low, the lack of bonding could mean that the HiPIC composites slip at low stress levels. Since interfacial slip is strain amplitude dependent, the strain amplitude dependency of the composites and the monolithics of this investigation was determined. Other researchers indicate at least a weak strain amplitude dependence for similar continuous fiber composites [11,37]. It is generally acknowledged that the damping of alloyed metals or heavily cold worked metals is strain amplitude dependent at levels greater than 10^{-4} or 10^{-5} [2]. It was determined that the strain amplitudes achieved in this investigation were on the order of 10^{-8} to 10^{-9} for the 7% Gr(p-r)/Al in the first mode. It is therefore safe to conclude that the monolithic materials exhibit strain amplitude independent damping. A linearity test was performed on the 7% Gr(p-r)/Al for mode 1 to determine if the composites were strain amplitude sensitive. The results are pictured in Figure 4.17. The loss factors in Figure 4.17 have an error of 4.11%. This lies well within the experimental error of 10.9% indicating that the MMCs are also in a strain amplitude independent regime. The strain amplitude independence is most likely attributable to the low strain amplitudes achieved in this investigation. It is unlikely that the mechanism responsible for the enhanced damping of the continuous fiber reinforcements over discontinuous reinforcements is interfacial slip because interfacial slip is a strain amplitude dependent mechanism. Other possible mechanisms include microplasticity at the interface, microcracking at or near the interface and intercrystalline thermal

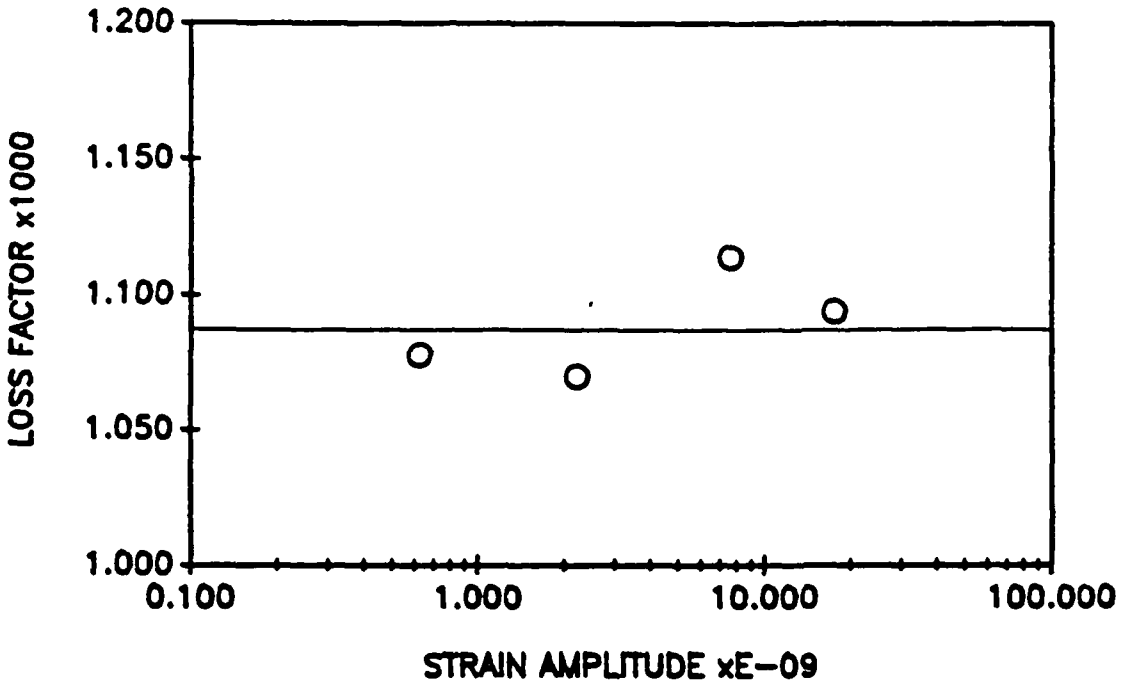

Figure 4.17 Plot showing strain amplitude independence (within the limits of experimental error) for the 7% Gr(p-r) composite

currents. Perhaps the damping mechanism is some sort of relaxation of thermal currents associated with heat flow between the matrix and the fiber, as opposed to heat flow between the different grains. This seems plausible since strain gradients exist between the fiber and the matrix and since reinforcements smaller than the load transfer length would not develop as large a strain gradient.

The damping data for the Gr(p-r)/Al composites is presented in Figure 4.18 along with the reference aluminum data. It is observed that significant improvements in damping have been achieved by the reinforcement with planar random graphite fibers. It is also interesting to note that a 6061 Al specimen which was made by the HiPIC technique which contains no reinforcement also shows enhanced damping. The transverse thermal current relaxation accounts for only a small fraction of the damping of any of the HiPIC specimens. Clearly, there is some sort of significant mechanism which is enhancing the damping of these composites. Comparison of mode 2 data referenced to the 6061-T6 Al shows that the unreinforced casting, the 7% Gr(p-r) casting, the 15% casting, and the 27% casting have 13.2, 12.5, 8.2 and 14.1 times the damping of the aluminum, respectively. The unreinforced casting appears to have a large relaxation below 1 kHz due to the steep slope of the curve. The grain size of the cast unreinforced aluminum was measured to be about 0.75 mm. Using equation (4.4), this corresponds to an intercrystalline thermal current relaxation maximum at about 580 Hz. This additional relaxation is most likely responsible for the enhanced damping of the unreinforced specimen. Similar calculations for the reinforced planar random composites reveal that, based upon their grain

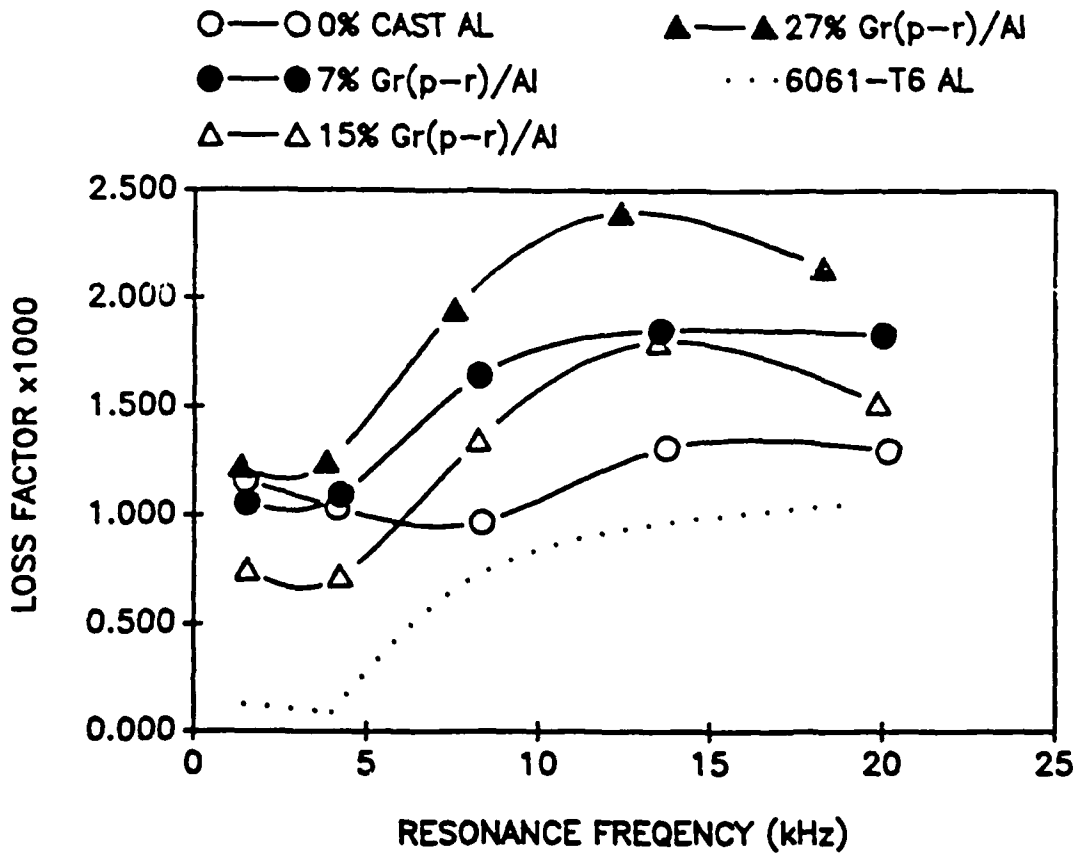

Figure 4.18 Plots of the loss factor of the 0%, 7%, 15% and 27% Gr(p-r)/Al composites and wrought 6061-T6 Al

sizes, their intercrystalline thermal current maxima should occur at 6700 Hz, 8700 Hz and 8100 Hz for the 7%, 15% and 27% composites, respectively. The calculation of the maximum of the relaxation was performed by using thermodynamic properties for the composite based upon a rule-of-mixture. While the use of a rule-of-mixtures relation is a rough approximation for the actual thermodynamic properties of the material, it partially accounts for the presence of the graphite fibers in the aluminum matrix.

4.3 Improved Damping by the Extrinsic Approach

4.3.1 Monolithic Substrate Study

The monolithic substrate study consisted of analyzing the improvements in damping induced by the application of coatings of high damping metals. 6061-T6 Al was chosen as the substrate material for the coatings. The coatings were applied to the substrates by a technique known as plasma spraying. Plasma spraying, as its name implies, is achieved by injecting powders of the material which is to be sprayed into a plasma stream of inert gasses. The plasma is created by the application of a large currents through the gasses which are then superheated. The powder becomes molten and cools rapidly upon contact with the substrate. Powders of incramute and nitinol were applied to the substrates. The damping of incramute and nitinol as measured in this investigation are shown in Figure 4.19. It is at first alarming that the damping of these two high damping alloys could be as low as

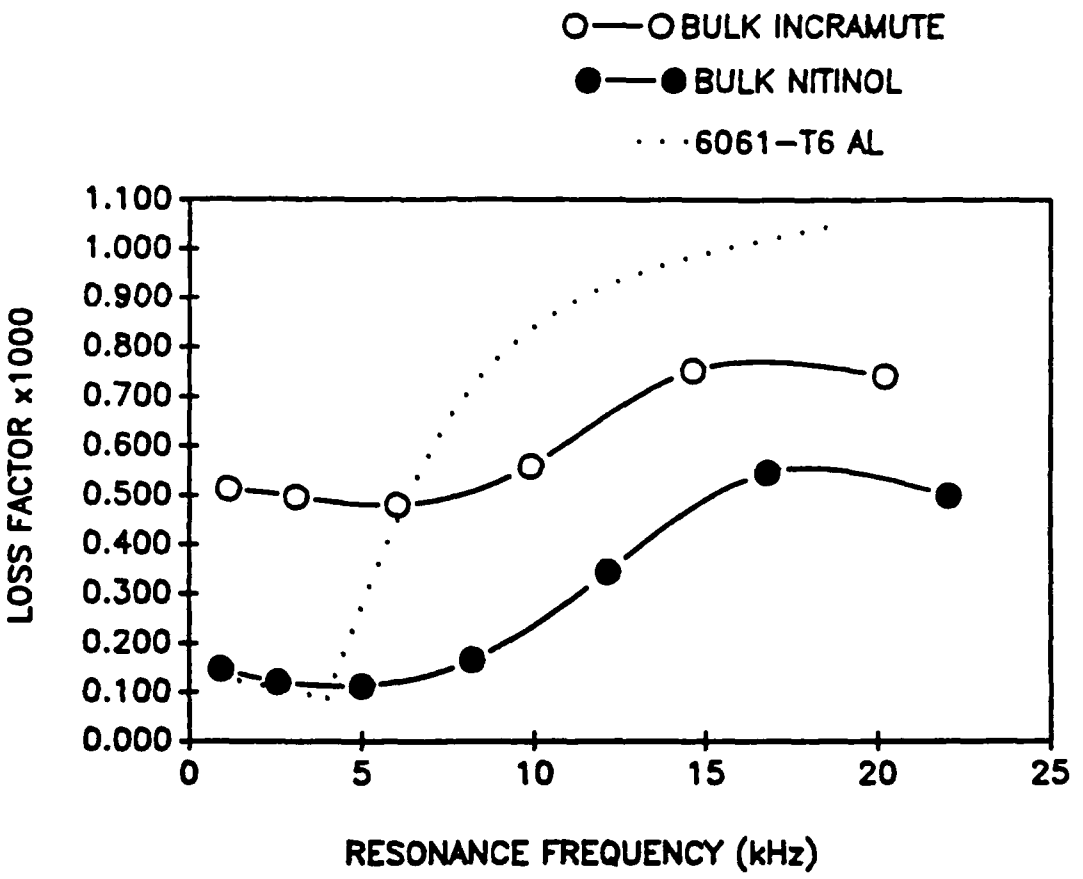

Figure 4.19 Plots of the loss factor of bulk nitinol and bulk incramute and wrought 6061-T6 Al

aluminum. However, these materials were described earlier as possessing non-linear damping mechanisms which are strain amplitude dependent. These mechanisms aren't activated until strain amplitude on the order of 10^{-6} are achieved. Therefore, the low measured damping of these high damping alloys is due to the low strain amplitudes to which the experimental setup is limited to. Another possible explanation for the low damping of the high damping alloys is that their heat treatment condition is not known. Therefore, the high damping alloys could be in a state which is far from the peak damping heat treatment. The powders of each of the two high damping alloys were tested in different forms, unalloyed and prealloyed. The unalloyed powders were prepared by ball milling elemental powders of the two materials resulting in a mechanical mixture of the two components. Prealloyed powders were obtained which have a more homogenous microstructure since the powders are made from the alloy itself. The powders were applied in varying thickness up to 400 μm per side. The 6061-T6 Al substrates were suitably undersized so that the coated specimens would all have the same approximate dimensions. The loss factor versus coating thickness of unalloyed incramute has been plotted for mode 1 in Figure 4.20. It is seen that a near linear curve results. The coating provides about 27.5 times the damping of the aluminum substrate for the 400 μm coating based on the first mode damping values. The damping from Figure 4.20 should not contain the effects of air damping since the data is measured below coincidence. However, the data of Figure 4.20 could be affected by the relative amounts of transverse thermal current relaxation. The increase in density due to coating thickness is plotted in Figure 4.21. The 400

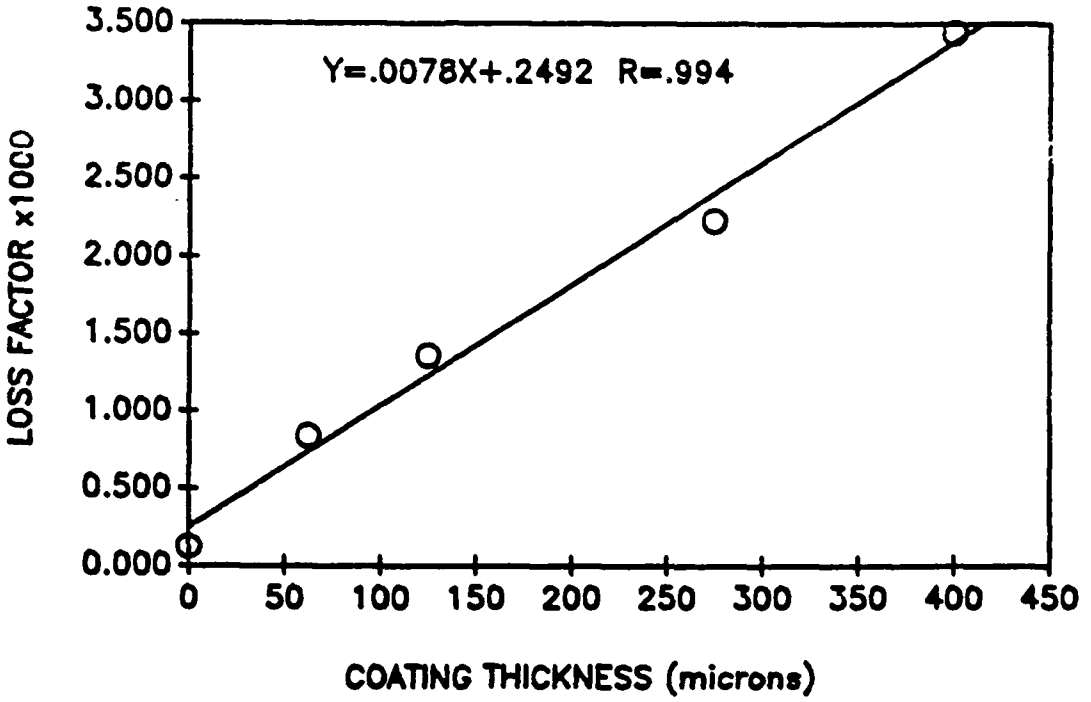

Figure 4.20 Plot of the loss factor as a function of coating thickness of unalloyed incramute on 6061-T6 Al (for mode 1)

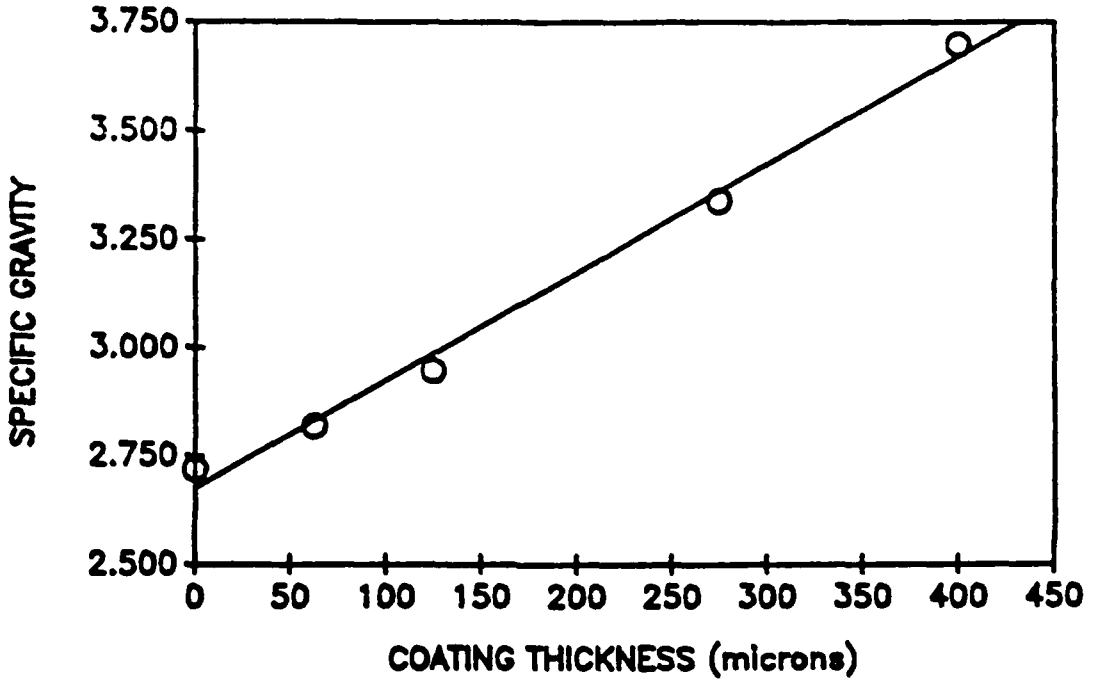

Figure 4.21 Plot of the specific gravity as a function of coating thickness of unalloyed incramute on 6061-T6 Al

μm per side coating is 1.36 times the density of the substrate. Therefore, there is a definite tradeoff between density and damping by the use of coatings. The effect of the alloy condition of the powders is pictured in Figure 4.22. Evidently, the condition of the powders does not have much effect on the measured damping. The coatings provide about 25 times the damping of the aluminum substrate irrespective of the alloy condition of the powder or even of the type of high damping alloy which was used. It is interesting to notice that the coated specimens exhibit much higher damping than the pure coating materials themselves. One explanation may lie in the large residual stresses which are developed in the specimens during the coating procedure. During plasma spraying, a large and rapid temperature drop occurs when the liquid metal quenches on the specimen surface. The coating materials have lower coefficients of thermal expansion than the aluminum substrates. Consequently, large residual stress build up in the specimen. The stresses are compressive in the coating and tensile in the substrate. The residual stresses caused warpage of the specimens when the coating was as low as one tenth of the substrate thickness. The layers were applied incrementally while flipping the specimens over in the hope of preventing warpage but this was ineffective. It is possible that the large compressive residual stress is either providing a damping mechanism or is enhancing a damping mechanism which already exists to provide the high measured damping. It is also possible that the grain size of the coating is such that intercrystalline thermal current relaxation is occurring. It again must be mentioned that these specimens are well below the regime for which the high damping

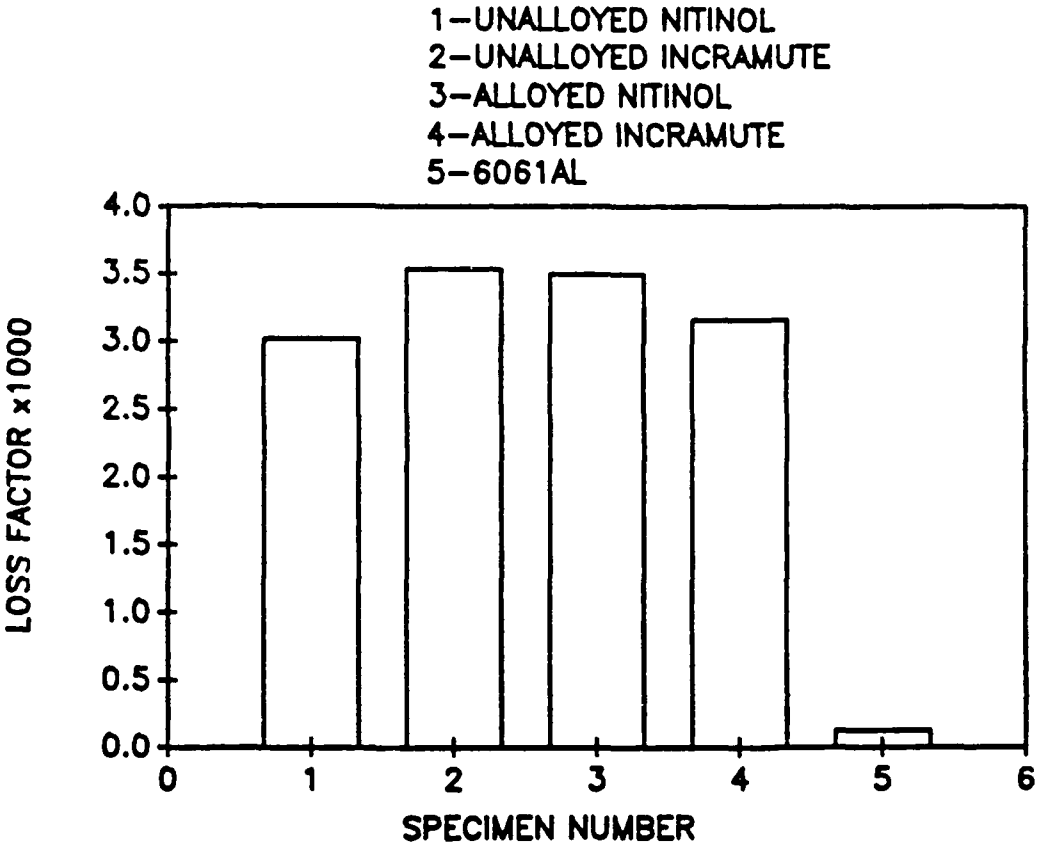

Figure 4.22 Comparison of the effects of coating alloy condition on the loss factor (for mode 1)

mechanisms are active. It is likely that if strain amplitudes were encountered such that the high damping mechanisms became activated, the prealloyed powders would show significant improvements over the unalloyed powders.

4.3.2 MMC Substrate Study

A coating of unalloyed incramute was applied to an $Al_2O_3(p)/Al$ substrate. The coating was to be 400 μm per side but only 180 μm per side was applied due to technical difficulties. The substrate had been undersized so that a 400 μm per side coating would make the specimen as thick as the uncoated aluminum, the intended thickness of all the coated specimens. In order to compensate for this, the damping value of a 180 μm per side coating of unalloyed incramute on aluminum was extrapolated from Figure 4.20. This value has been plotted along with the measured value for the coated $Al_2O_3(p)/Al$ substrate in Figure 4.23. No significant difference is observed between the two substrates. The difference which does exist between the two substrates could be caused in part by the fact that the $Al_2O_3(p)/Al$ substrate has a lower ratio of coating to substrate since it was undersized for a 400 μm coating.

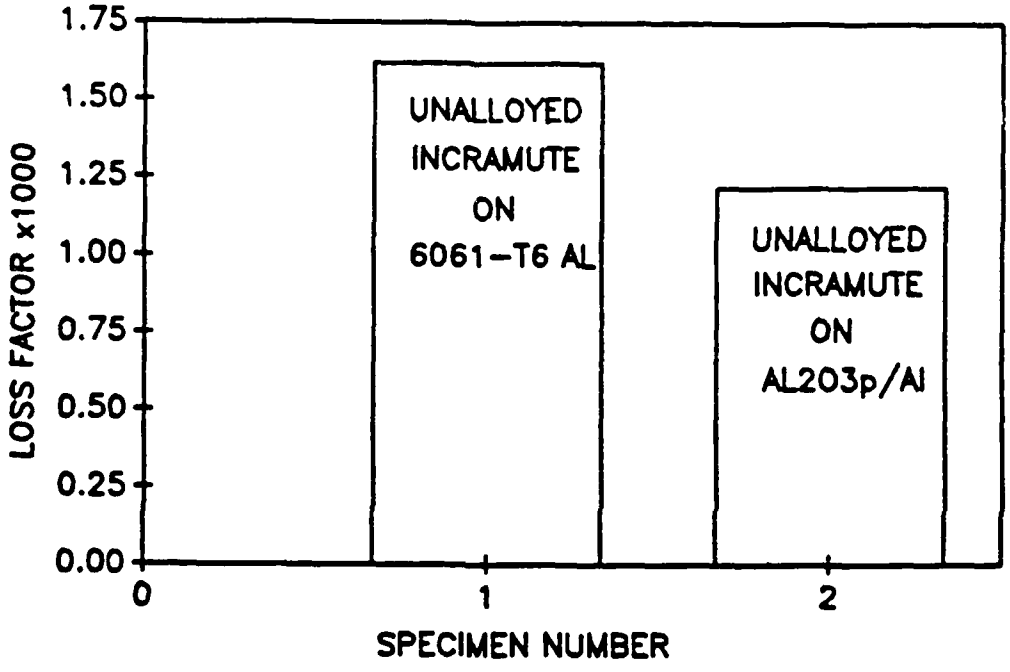

Figure 4.23 Comparison of loss factor for substrates of wrought 6061-T6 Al and Al_2O_3(p)/Al coated with unalloyed incramute (for mode 1)

Chapter 5

SUMMARY AND CONCLUSIONS

A series of materials have been evaluated for their tensile stiffness, strength and damping performance. These include Al-Mg (MA), SiC_p/Al-Cu (MA), SiC_p/Al, Al_2O_3(p)/Al, SiC_w/Al, Gr(planar-random)/Al, unidirectional Gr/Al and unidirectional SiC/Al composites. The damping performance was also measured for coatings of incramute and nitinol (both unalloyed and prealloyed powders), bulk incramute and bulk nitinol. All of the continuous fiber composites were manufactured by high pressure infiltration casting (HiPIC). The damping measurements have been carried out at room temperature in air with a laser vibrometer over a frequency range from .7 kHz to 25.6 kHz at low strain amplitudes (10^{-10} to 10^{-7}). 6061-T6 Al shows transverse thermal current relaxation but little or no intercrystalline thermal current relaxation.

The mechanically alloyed materials have only marginally improved damping compared to 6061-T6 Al after the effects of transverse thermal current relaxation are considered. No difference is observed between the unreinforced Al-Mg (MA) and the SiC_p/Al-Cu (MA). The particulate reinforced composites have approximately the same damping as the 6061-T6 Al after the effects of transverse thermal current relaxation are considered. The transverse thermal current relaxation is specimen dimension dependent and is more significant for thin specimens. The SiC_w/Al composite has the same damping as the 6061-T6 Al.

The continuous fiber composites (both unidirectional and planar random) show enhanced damping relative to 6061-T6 Al. The

unidirectional SiC/Al and the unidirectional Gr/Al composites show 5 and 4 times the damping of 6061-T6 Al, respectively. The planar random Gr/Al composites show damping of 13.2, 12.5, 8.2 and 14.1 times that of the 6061-T6 Al for the 0%, 7%, 15% and 27% fiber volume fraction castings, respectively. The enhanced damping of these composites is attributed to the relaxation of intercrystalline thermal currents. It is suggested that the enhanced damping of the continuous fiber composites is due to a relaxation of thermal currents which flow between the fiber and the matrix as a result of the strain gradient inherent to the continuous fiber composites.

The loss factors of incramute and nitinol are on the same order as the 6061-T6 Al under the low strain amplitudes of this investigation. Apparently, the strain amplitude dependent mechanisms responsible for the high damping of these materials are not activated at the low strain amplitudes. The coated specimens show that damping is approximately linear with coating thickness and otherwise independent of the alloyed condition of the coating. An incramute coating of about 0.4 mm on each side of aluminum beam specimens shows a damping which is about 25 times that of 6061-T6 Al. Compressive residual stresses in the coatings may be responsible for the enhanced damping of the coated specimens over that of the bulk coating alloys.

Chapter 6

RECOMMENDATIONS FOR FUTURE WORK

Effects of air damping can be minimized by performing the damping measurement in a vacuum chamber. It would also be desirable to control the temperature of the chamber. This would allow the measurement to be performed at a specific frequency but for a range of temperatures. A fixed frequency test could be performed by exciting the same mode and would eliminate the need to reposition the supports at the nodes for different modes. This would reduce the time required to perform a test since the chamber would have to be evacuated only once for a desired measurement. The above test setup would also help to reduce specimen geometry effects on the damping.

The specimens which were evaluated in this investigation were all tested in as-received condition. Heat treatment of the MMCs could improve both damping characteristics and tensile test properties. Further, the coating materials could show significant improvements in damping if they are aged under optimum conditions of temperature and time to achieve peak damping. Another technique would be to combine the intrinsic and extrinsic approaches to improved damping by fabricating composites from fibers which have been coated with a suitable high damping alloy. This hybrid technique could be significant since the coating would be at the interface of the composite and because composites have inherently large strains at the interface. These large strains could help to activate the strain amplitude dependent mechanism of the high damping coating materials. Further, composites utilizing

this hybrid approach could be fabricated by the HiPIC technique, which leaves fiber coatings intact.

REFERENCES

1. Chawla, K.K., Composite Materials. Ilschner, B. and Grant, N.J., editors, Springer-Verlag, New York, 1987.

2. Norwick, A.S., and Berry, B.S., "Anelastic Relaxation in Crystalline Solids," Academic Press, New York, 1972.

3. Ray, A.K., Wren, G.G., and Kinra, V.K., "Comparison of Experimental Techniques in the Measurement of Damping Capacity of Metal-Matrix Composites," Department of Aerospace Engineering and Mechanics and Materials Center, Texas A&M University, College Station, Texas, 1985.

4. Zener, C., Elasticity and Anelasticity of Metals. The University of Chicago Press, Chicago, 1948.

5. Nashif, A.D., Jones, D.I.G., and Henderson, J.P., Vibration Damping. John Wiley & Sons, New York, 1985.

6. De Batist, R., Internal Friction of Structural Defects in Crystalline Solids, Amelinckx, S., Gevers, R., and Nihoul, J., editors, American Elsevier Publishing Company, Inc., New York, Vol. 5, 1972.

7. Humbeeck, J.V., "High Damping Capacity Due to Microstructural Interfaces," Role of Interfaces on Material Damping, Proceedings of an International Symposium held in conjunction with ASM's Materials Week and TME/AIME Fall Meeting, Toronto, Ontario, Canada, Oct. 13-17, 1985.

8. Bert, C.W., "Composite Materials: A Survey of the Damping Capacity of Fiber Reinforced Composites," ASME Winter Meetings 1980 Proceedings.

9. DiCarlo, J.A., and Maisel, J.E., "High Temperature Dynamic Modulus and Damping of Aluminum and Titanium Matrix Composites," Advanced Fibers and C[illegible]posites for Elevated Temperatures, Ahmad, I. and Noton, B.R., e[illegible]tors, Proceedings of a symposium sponsored by The Metallurgical Society of AIME and American Society for Metals Joint Composite Materials Committee at the 108th AIME Annual Meeting, New Orleans. Louisiana, Feb. 20-21, 1979.

10. Bhagat, R.B., Amateau, M.F., and Smith, E.C., "Logarithmic Decrement Measurements on Mechanically Alloyed Aluminum and SiC Particulate Reinforced Aluminum Matrix Composites," Cast Reinforced Metal Composites. S.G. Fishman and A.K. Dhingra, editors. Proceedings of the International Symposium on Advances in Cast Reinforced Metal Composites held in conjunction with the 1988 World Materials Congress, Chicago, Illinois, Sept. 24-30, 1988.

11. Rawal, S.P., and Misra, M.S., "Interfaces and Damping in Continuous Gr/Al Composites," Role of Interfaces on Material Damping, Proceedings of an International Symposium held in conjunction with ASM's Materials Week and TMS/AIME Fall Meeting, Toronto, Ontario, Canada, Oct. 13-17, 1985.

12. DiCarlo, J.A., and Maisel, J.E., "Measurement of the Time-Temperature Dependent Dynamic Mechanical Properties of Boron/Aluminum Composites," American Society for Testing and Materials, 1916 Race St., Philadelphia, PA 19103, 1979.

13. Wren, G.G., and Kinra, V.K., "An Experimental Technique for Determining a Measure of Structural Damping," Journal of Testing and Evaluation, JTEVA, **16**, No. 1, Jan. 1988, pp. 77-85.

14. Ni, R.G., and Adams, R.D., "The Damping and Dynamic Module of Symmetric Laminated Composite Beams--Theoretical and Experimental Results," Journal of Composite Materials, **18**, March 1984, pp. 104-121.

15. Rohatgi, P.K., Asthana, R., and Kumar, A., "Damping Capacity of Aluminum Alloy Matrix Composites," Cast Reinforced Metal Composites, S.G. Fishman and A.K. Dhingra, editors. Proceedings of the International Symposium on Advances in Cast Reinforced Metal Composites held in conjunction with the 1988 World Materials Congress, Chicago, Illinois, Sept. 24-30, 1988.

16. Crawley, E.G., Sarver, G.L., and Mohr, D.G., "Experimental Measurement of Passive Materials and Structural Damping for Flexible Space Structure," in Vibration Damping-1984, (Workshop Proc.), AFWAL-TR-84-3064, A-23.

17. Lee, G.F., and Anderson, C.W., "Vibration Damping Workshop Proceedings," Naval Weapons Center, Long Beach, CA, Feb. 1984, AD-P004, 703/5/WMS, Nov. 1984.

18. Kishore, N.N., Ghosh, A., and Agarwal, B.D., "Damping Characteristics of Fiber Composites with Imperfect Bonding Part I--Low Volume Fraction Composites," Journal of Reinforced Plastics & Composites, Vol. 1 (January 1982), pp. 40-63.

19. Kishore, N.N., Ghosh, A., and Agarwal, B.D., "Damping Characteristics of Fiber Composites with Imperfect Bonding Part II--Low Volume Fraction Composites," Journal of Reinforced Plastics & Composites, Vol. 1 (January 1982), pp. 64-81.

20. Töpler, J., and Arnhold, V., "Damping Properties of P/M Aluminum Alloys," The International Journal of Powder Metallurgy, **25**, No. 2, 1989.

21. Bhagat, R.B., Amateau, M.F., and Smith E.C., "Damping Behavior of Squeeze Cast Planar Random Carbon Fiber Reinforced 6061 Al Matrix Composites," Cast Reinforced Metal Composites, Fishman, S.G. and Dhingra, A.K., editors, Proceedings of the International Symposium on Advances in Cast Reinforced Metal Composites held in conjunction with the 1988 World Materials Congress, Chicago, Illinois, Sept. 24-30, 1988.

22. Cronauer, J.T., "A Comparison of High Damping Shape Memory Alloys with Cu-Mn-Based and Fe-Cr-Based Alloys," Thesis, Naval Postgraduate School, 1987.

23. Luxon, J.T., and Parker, D.E., Industrial Lasers and Their Applications. Prentice-Hall, Inc., Englewood Cliffs, NJ, 1985.

24. Maksimov, Y.F., Novikov, I.I., and Proskurin, V.B., "Effect of Natural Aging on Internal Friction in A Cu-Mn Metalloceramic Alloy," UDC 669.35'74:539.67.

25. Sample, R.J., Bhagat, R.B., and Amateau, M.F., "High Pressure Squeeze Casting of Unidirectional Graphite Fiber Reinforced Aluminum Matrix Composites," Cast Reinforced Metal Composites, Fishman, S.G. and Dhingra, A.K., editors, Proceedings of the International Symposium on Advances in Cast Reinforced Metal Composites held in conjunction with the 1988 World Materials Congress, Chicago, Illinois, Sept. 24-30, 1988.

26. Benjamin, J.S. and Volin, T.S., Metall. Trans., 5, 1929, 1974

27. Read, B.E., and Dean, G.D., The Determination of Dynamic Properties of Polymers and Composites. Adam Hilger, Bristol, England, 1978.

28. Junger, M.C., and Feit, D., Sound Structures, and Their Interaction. 2nd Edition, Massachusetts Institute of Technology Press, Cambridge, MA, 1986.

29. Conversation with Eugene Skudrzyk, Aug. 1989.

30. Skudrzyk, E., Simple and Complex Vibratory Systems. The Pennsylvania State University Press, University Park, PA, 1981.

31. Blake, W.K., "Radiation from Free-Free Beams Under Influences of Light and Heavy Fluid Loading," Naval Ship Research and Development Center report 3716, Bethesda, MD, 1971.

32. Berry, B.S., J. Appl. Phys., 26, 1221, 1955a.1.

33. Wren, G.G., and Kinra, V.K., "On the Effect of an End-Mass on Beam Damping," to be published.

34. Randall, R.H., Rose, F.C., and Zener, C., Phys. Rev., **56**, 343, 1939.

35. Entwistle, K.M., J. Inst. Metals, **75**, 97, 1948.

36. Kerlin, R., "Interval Frictions Studies on Bell Metal and Wood," File No.: 603.2811, March 14, 1966.

37. Wren, G.G., and Kinra, V.K., "An Experimental Study of the Complex Dynamic Modulus," Dynamic Elastic Modulus Measurements in Materials, ASTM STP 1045, Alan Wolfenden, editor, American Society for Testing and Materials, Philadelphia, 1989.

Appendix A

CALCULATION OF RELAXATION TIME AND STRENGTH OF TRANSVERSE THERMAL CURRENTS FOR 6061-T6 Al

6061-T6 Al has the following properties:

C_p = 896 J/Kg-K

k_t = 167 W/m-K

α = 23.6 μm/m-K

ρ = 2700 Kg/m ^{3}

The relaxation strength of transverse thermal currents can be calculated from these data as follows:

$$\eta_{o_{TTC}} = \frac{\alpha^2 ET}{\rho C_P} = 4.639 \times 10^{-3}$$

The wrought 6061-T6 Al specimen is 2.79 mm thick (h = 2.79 mm). Using this, the relaxation time can be calculated:

$$\tau_{TTC} = \frac{h^2 \rho C_P}{\pi^2 k_t} = 11.42 \times 10^{-3} \text{ sec}$$

Note that the relaxation strength is specimen independent while the relaxation time is specimen dependent.

Appendix B

CALCULATED DAMPING FROM THE SUPERPOSITION OF TWO RELAXATIONS

The plot of the calculated damping in Figure 4.7 was generated by plotting η_{total} as given by the equation below:

$$\eta_{o_{TOTAL}} = \eta_{o_{TTC}} \frac{\omega\tau_{TTC}}{1+(\omega\tau_{TTC})^2} + \eta_{o_{ICTC}} \frac{\omega\tau_{ICTC}}{1+(\omega\tau_{ICTC})^2}$$

This equation assumes that the experimentally measured damping is due to the superposition of the relaxation of transverse thermal currents and the relaxation of intercrystalline thermal currents. Values for η_{oTTC}, τ_{TTC} and τ_{ICTC} can be calculated with reasonably accuracy using the equations given in Chapter 4. However, η_{oICTC} can not be calculated with any accuracy. Calculated values for η_{oICTC} are typically an order of magnitude greater than experimentally measured values. Therefore, an estimate of η_{oICTC} must be obtained from some other means. The theoretical damping contribution of a relaxation must be a lower bound on the experimentally measured damping. Therefore, an estimation of η_{oICTC} can be obtained by solving for η_{oICTC} from the above equation when η_{total} is set to the lowest experimentally measured damping value:

$$\eta_{o_{ICTC}} = \left(\eta_{o_{TOTAL}} - \eta_{o_{TTC}} \frac{\omega\tau_{TTC}}{1+(\omega\tau_{TTC})^2} \right) \frac{1+(\omega\tau_{ICTC})^2}{\omega\tau_{ICTC}}$$

By setting η_{total} equal to the lowest experimentally measured value, the requirement that the theoretically calculated relaxation damping must be a lower bound is satisfied. In this manner, an estimate of the intercrystalline thermal current relaxation strength can be obtained. This method of estimating η_{oICTC} neglects all other sources of damping i.e. damping mechanisms other than transverse thermal current relaxation, intercrystalline thermal current relaxation and extraneous damping.

Appendix C

HIGH FREQUENCY AIR DAMPING

Due to the difficult integral equations which result in the derivation of the radiation resistance, exact solutions do not exist near coincidence. However, it is known that the radiation resistance does approach a constant value at a sufficiently high frequency above coincidence. Unfortunately, it is not possible to predict the exact frequency above coincidence where the radiation resistance becomes constant. Figure C-1 presents actual experimental data in addition to the calculated air damping due to radiation assuming the radiation resistance has become constant. From Figure C.1, it is seen that the calculated air damping decreases with increasing frequency. This is due to the inverse frequency dependence that air damping possesses. Steel shows evidence that the radiation resistance is constant for modes 4 and 5. Aluminum, however, does not seem to be following this trend in the high frequency limit, at least not for the frequency range of this investigation. Blake [31] performed actual sound radiation measurements on steel and aluminum and also found that steel approaches constant radiation resistance more quickly than does aluminum.

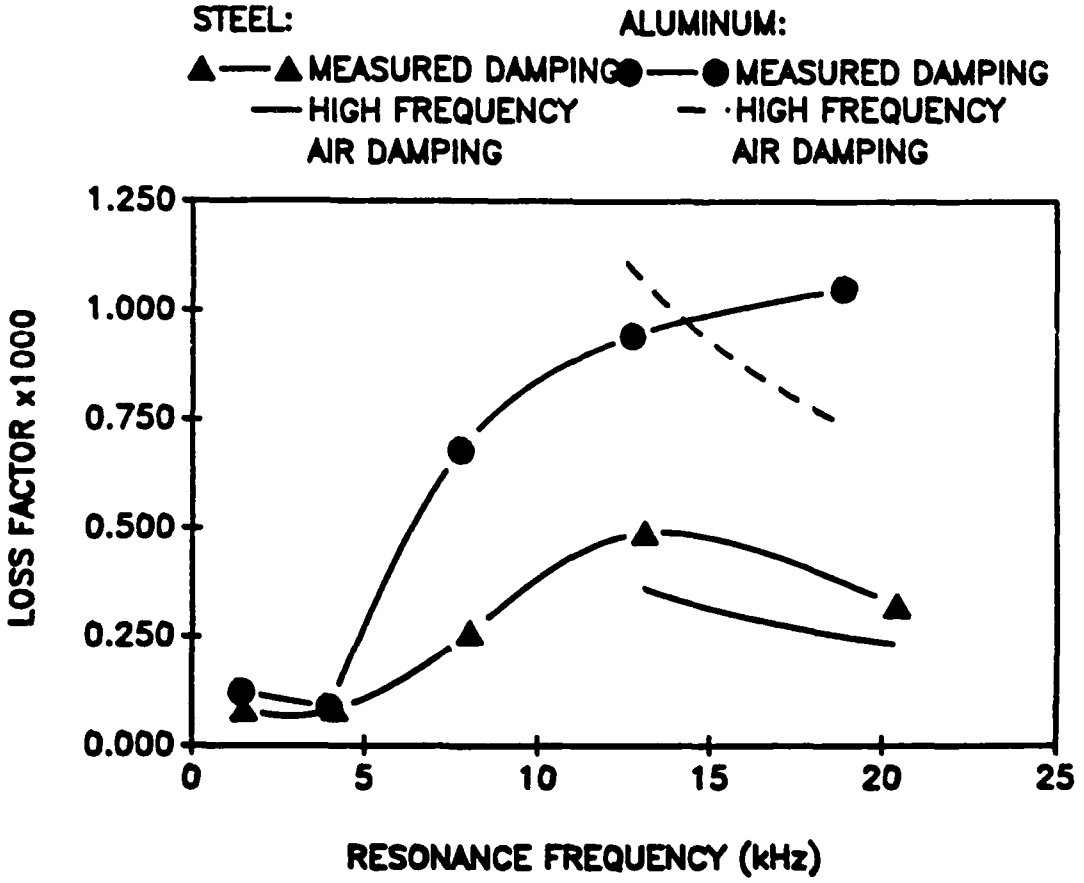

Figure C-3 Proposed theoretical high frequency limit air damping and actual experimentally measured damping for wrought 6061-T6 Al and a plain low carbon steel

The Pennsylvania State University
Applied Research Laboratory
P.O. Box 30
State College, PA 16804